STOPPING CROSS-SECTIONS IN BORON OF LOW-ENERGY ATOMS WITH $Z \leq 11$

STOPPING CROSS-SECTIONS IN BORON OF LOW-ENERGY ATOMS WITH $Z \leq 11$

By

James Robert Macdonald, B.A.

A Thesis

Submitted to the Faculty of Graduate Studies

in Partial Fulfilment of the Requirements

for the Degree

Master of Science

McMaster University

October 1964

MASTER OF SCIENCE (1964)
(Physics)

McMASTER UNIVERSITY
Hamilton, Ontario.

TITLE: Stopping Cross-Sections in Boron of Low-Energy Atoms with $Z \leq 11$.

AUTHOR: James Robert Macdonald, B.A. (University of Toronto)

SUPERVISOR: Professor H.E. Duckworth

NUMBER OF PAGES: vii, 39.

NUMBER OF FIGURES: 26

SCOPE AND CONTENTS: This thesis is concerned with the energy loss of light atomic projectiles in thin boron films. In Chapter I, a brief theoretical description of the stopping process is given. In Chapter II, the experimental procedure is described and a method is given by which electronic stopping cross-sections can be determined from the observed energy loss. In Chapter III, the thin boron films that are used in the experiments are described in detail. In Chapter IV, the experimental results are presented, and in Chapter V the results are compared with existing data and theory.

ACKNOWLEDGEMENTS

The guidance and encouragement of my supervisor, Professor H.E. Duckworth, during the course of this work was greatly appreciated.

I would like to thank Dr. D.B. McLean for the use of his microbalance, Dr. R.K. Ham and Mr. H. Walker for their assistance in the use of the electron microscope, and Dr. J.H. Ormrod for kindly assisting me with the Monte Carlo computer calculation. I am most grateful to Mr. Paul Van Rookhuyzen for his assistance with technical problems and for his work in the preparation of this thesis. Discussions with Dr. J.H. Ormrod and Dr. R.C. Barber were invaluable stimuli during the course of these experiments.

Financial assistance from the Province of Ontario, the National Research Council, and the McMaster University Department of Physics is gratefully acknowledged.

This research was supported by grants from the National Research Council of Canada and by the United States Air Force Office of Scientific Research.

TABLE OF CONTENTS

	Page
Chapter I - INTRODUCTION	1
1. Background	1
2. Theoretical Approach to the Stopping of Atomic Projectiles	2
3. Theory of the Electronic Straggling in Energy	8
Chapter II - APPARATUS AND DATA ANALYSIS	10
1. Apparatus	10
2. Experimental Procedure and Data Analysis	12
Chapter III - THIN FILMS	18
1. Production of the Films	18
2. Thickness of the Boron Films	19
3. Quality of the Boron Films	23
Chapter IV - EXPERIMENTAL RESULTS	25
1. Stopping Cross-Sections	25
2. Straggling	27
Chapter V - DISCUSSION	31
1. Comparison with Other Experiments	31
2. Comparison of Stopping Cross-Sections with Theory	31
3. Comparison of Straggling with Theory	35
4. Summary	36
REFERENCES	38

LIST OF FIGURES

Following Page

Figure for Chapter I 9

Fig. 1. Universal Nuclear Stopping Cross-Section of Lindhard et al (L-63).

Figures for Chapter II 17

Fig. 2. Schematic Diagram of the Apparatus.

Fig. 3. Energy Spectra at an Average Energy of 37.6 keV for $H^1 \rightarrow$ Boron, and $Ne^{20} \rightarrow$ Boron.

Fig. 4. Energy Spectra for $Ne^{20} \rightarrow$ Boron at Average Energies of 25 keV and 60 keV.

Fig. 5. Angular Distribution of Ne^{20} Ions Emerging from Boron at 25 keV.

Fig. 6. Angular Distribution of Ne^{20} Ions Emerging from Boron at 40 keV.

Fig. 7. Calculated and Experimental Energy Distributions of $Ne^{20} \rightarrow$ Boron at 25 keV.

Figures for Chapter III 24

Fig. 8. Photograph of the Apparatus Used for the Evaporation of Boron.

Fig. 9. Electron Micrograph of a Boron Film.

Fig. 10. Photograph of the Electron Diffraction Pattern Produced by a Boron Film.

Fig. 11. Electron Micrograph of a Nickel Film.

Fig. 12. Photograph of the Electron Diffraction Pattern Produced by a Nickel Film.

LIST OF FIGURES (Continued) Following Page

Figures for Chapter IV 30

Figures 13-22. Stopping Cross-Sections in Boron of Projectiles with $Z \leq 11$.

Fig. 23. Straggling of 25 keV Hydrogen Projectiles Plotted Against the Energy Loss in Boron Films of Various Thickness.

Figures for Chapter V 37

Fig. 24. Stopping Cross-Section of Hydrogen Projectiles at Velocities Corresponding to Proton Energies from 5 to 150 keV.

Fig. 25. Electronic Stopping Cross-Sections as a Function of the Atomic Number of the Projectile.

Fig. 26. Observed Stopping Cross-Section for $C^{12} \rightarrow$ Boron and $B^{11} \rightarrow$ Carbon.

LIST OF TABLES

		Page
Table III-1.	The Determination of the Absolute Stopping Cross-Section for 30 keV Protons in Boron.	22
Table IV-1.	Coefficients (k) and Exponents (P) for the Electronic Stopping Cross-Sections in Boron as Expressed in the Equation $S_e = kE^P$.	28
Table V-1.	Comparison Between Experimental and Theoretical Values of the Relative Straggling in Boron.	37

CHAPTER I

INTRODUCTION

1. Background

The energy loss of atomic particles in passing through matter has been a subject of interest for some time. The extensive work on the subject has been summarized by Whaling (W-58) and more recently by Northcliffe (N-63).

The small number of experiments performed with projectiles having energies less than 100 keV prompted such experiments to be carried out in this laboratory. Previous work in this field in this laboratory consists of the following:

(1) The energy loss of H^1 and He^4 atoms having energies less than 30 keV in traversing thin films of various materials was studied by Van Wijngaarden and Duckworth (W-62).

(2) The systematic determination of stopping cross-sections in carbon films of atoms with $Z \leq 12$ in the energy interval from 10-140 keV by Ormrod and Duckworth (O-63).

(3) The determination of stopping cross-sections in aluminum and nickel foils of atoms with $Z \leq 12$ and the extension of the work described in (2) to $Z \leq 19$, both in the energy interval from 10-140 keV by Ormrod, Macdonald and Duckworth (O-64).

These experiments have been found to be in satisfactory agreement with the theoretical work of Lindhard et al (L-54, L-61, L-63). However an interesting experimental phenomenon not accounted for by the theory was found. The magnitude of the electronic stopping cross-section was found to vary periodically with the atomic number of the projectile. Further experiments were then proposed in order to add to the systematic data concerning the slowing down in solids of projectiles with keV energies.

This thesis represents an experimental study of the energy loss in thin boron films of atomic projectiles with $Z \leq 11$ in the energy interval from 15-140 keV.

2. Theoretical Approach to the Stopping of Atomic Projectiles

When an atomic projectile slows down in encounters with the atoms of a stopping medium, two distinct collision processes occur. These we shall distinguish as nuclear and electronic collisions.

We can define a total stopping cross section (S) by the following relation:

$$S = S_\gamma + S_\varepsilon = -\frac{1}{N}\frac{dE}{dx} \qquad \text{I-1}$$

where the subscripts γ and ε represent the nuclear and electronic stopping components respectively. (This notation will be used throughout this thesis.)

N is the number of stopping atoms per unit volume

$-\frac{dE}{dx}$ is the stopping power.

In this section we shall summarize the theory of nuclear stopping and then do the same for electronic stopping. Theoretical expressions for S_ν and S_ϵ applicable to our experiments will be given.

First, in nuclear collisions, energy is lost elastically to the recoiling atoms of the stopping medium. In each such collision, the energy lost by the penetrating atom is given by

$$\Delta T_\nu = \frac{4 M_1 M_2}{(M_1+M_2)^2} E \sin^2 \frac{\theta}{2} \qquad \text{I-2}$$

where M is the atomic mass

θ is the relative angle of deflection

E is the energy of the projectile

ΔT_ν is the energy transfer in a nuclear collision.

Throughout this thesis, the subscripts 1 and 2 will represent the projectile and target atoms respectively.

A nuclear stopping cross-section can be determined by integrating equation I-2 over all angles.

$$S_\nu = \int_0^\pi \Delta T_\nu \, d\sigma(\theta) \qquad \text{I-3}$$

where $d\sigma(\theta)$ is the differential scattering cross-section.

At high energies, the colliding atoms can be approximated by point charges, and nuclear collisions are described by the well-known Rutherford scattering (R-11). However, at lower energies, the projectile atom would be surrounded by most of its planetary electrons, and the penetration into the electron cloud of a scattering atom would only be partial. Thus, electron screening must be taken into account to

describe nuclear collisions at these energies. The energy range of our experiments brings them into this category.

The first detailed study of nuclear stopping at low energies was made by Bohr (B-48). In describing atomic collisions Bohr used an exponentially screened coulomb potential.

$$P(r) = \frac{Z_1 Z_2 e^2}{r} \exp\left(-\frac{r}{a}\right) \qquad \text{I-4}$$

where $P(r)$ is the potential between two atoms separated by a distance r.

Z is the atomic number

e is the elementary charge

$a = .8853\, a_o \left(Z_1^{2/3} + Z_2^{2/3}\right)^{-\frac{1}{2}}$ is the screening parameter.

$a_o = \frac{\hbar^2}{me}$ is the first Bohr orbit in hydrogen.

In Bohr's original work the numerical factor in the screening parameter was not used, but all subsequent workers in this field have used the factor and it will be used in this thesis.

At this point, it is convenient to introduce a dimensionless energy variable ε, first used by Lindhard and Scharff (L-61).

$$\varepsilon = \frac{a}{b} \qquad \text{I-5}$$

where $b = \frac{Z_1 Z_2 e^2}{\frac{M_2}{M_1+M_2} E}$ is the distance of closest approach between a projectile of energy E and a scattering atom in the unscreened case.

In the region $\varepsilon \ll 1$ Bohr assumed that nuclear collisions could be described by isotropic scattering in the centre of mass system. This simple differential cross-section, gave a nuclear stopping cross-section independent of energy in this region.

With $\varepsilon > 1$, the transition between isotropic scattering and Rutherford scattering begins. Although Bohr did examine this region, we shall use the later approach of Lindhard et al (L-61, L-63) to describe the energy loss in nuclear collisions. This is the region in which all our experimental results lie. In fact, for projectiles stopping in boron, $\varepsilon = 1$ for hydrogen at 0.3 keV and for sodium at 15 keV. Both these energies are beyond the low energy limit of our experiments.

Everhart et al (E-55), Firsov (F-58), and Lindhard et al (L-61, L-63) have used a perturbation technique to calculate numerically the differential cross-section for a potential that includes electron screening. Everhart used the Bohr potential (equation I-4) while both Firsov and Lindhard used a coulomb potential screened by the Fermi function $\varphi_o\left(\frac{r}{a}\right)$.

The nuclear stopping cross-section was calculated by Lindhard from the differential cross-section, by performing the integration of equation I-3 numerically. The stopping cross-section so obtained is applicable to all projectile-target combinations and is shown in Fig. 1. Here the reduced stopping power $\frac{d\varepsilon}{d\rho}$ is plotted against $\varepsilon^{\frac{1}{2}}$, where ε is given in equation I-5 and

$$\frac{d\varepsilon}{d\rho} = \frac{M_1 + M_2}{M_1} \cdot \frac{1}{4\pi e^2 Z_1 Z_2 a} \cdot S_v \qquad \text{I-6}$$

Next, we shall consider the energy lost by atomic projectiles to the electrons of the stopping medium.

At high energies, the electronic stopping cross-section is given by the familiar formula $S_e \propto \frac{1}{E} \ln E$ due to Bloch (B-33). This expression was derived using the approximation that the electrons were stationary in the stopping medium. In our experiments, the Bloch formula is not valid, since the projectile velocity is the same order of magnitude as the electron velocity. For example, v_o, the velocity in the first Bohr orbit is attained at a hydrogen ion energy of 25 keV.

Fermi and Teller (F-47)have calculated the energy loss of low energy mesons and their argument is applicable to heavier projectiles as well. The stopping medium is approximated by a degenerate electron gas in which the maximum electron velocity is v_M. When energy is transferred to the electrons, the amount transferred per collision is of the same order as the velocity v of the penetrating projectile. Because of the Pauli exclusion principle, all collisions are forbidden for which the final velocity of the electron lies inside the velocity space of the degenerate electron gas. Thus, only those electrons with speeds close to v_M by amounts of the order v will be available to undergo collisions. Their number will be proportional to v. Since the average energy exchange is also proportional to v, the rate of energy loss will be given by

$$\frac{dE}{dt} \propto v^2 \qquad \text{I-7}$$

and hence the stopping power is

$$-\frac{dE}{dx} \propto v \qquad \text{I-8}$$

Using an extension of the above argument, based on the Thomas-Fermi model of the atom, Lindhard and Scharff (L-61) have developed the following expression for the electronic stopping cross-section:

$$S_\varepsilon = \xi_\varepsilon \cdot 8\pi e^2 Z_1 Z_2 (Z_1^{2/3} + Z_2^{2/3})^{-3/2} a_o \frac{v}{v_o} \qquad \text{I-9}$$

for $v < v_o Z_1^{2/3}$.

where $v_o = \frac{e}{\hbar^2}$ is the velocity in the first Bohr orbit of hydrogen.

ξ_ε is of the order $Z_1^{1/6}$.

From a consideration of S_γ given in Fig. 1 and S_ε given in equation I-9, we see that the nuclear contribution to the stopping process will decrease while the electronic component will increase with the energy of the penetrating particle.

We find that our experimental cross-sections can be compared directly with equation I-9 when the contribution of S_γ is removed by a Monte Carlo calculation developed by Ormrod (O-63) and described in the following chapter.

3. Theory of the Electronic Straggling in Energy

When the projectiles pass through a film, a distribution in energy arises amongst them for two reasons. First, the various particles undergo different numbers of collisions in traversing the film. Second, the energy transfer per collision is not the same for all collisions. The distribution in energy among the projectiles is commonly called the straggling in energy of the projectiles (L-54).

Lindhard (L-54) has examined the straggling of a beam of atoms losing energy to electronic processes in a solid. By replacing the solid by a degenerate electron gas, Lindhard obtained the following estimate of the relative electronic straggling of low velocity atoms:

$$\frac{\Omega_\varepsilon^2}{\Delta E} \simeq \left[5 m v^2 \hbar \omega_o\right]^{\frac{1}{2}} \qquad \text{I-10}$$

where Ω_ε is the standard deviation of the energy distribution of the atoms after passing through the solid.

ΔE is the most probable energy loss.

(For the symmetric distributions involved with electronic stopping processes, ΔE is also the average energy loss.)

$\hbar$ is Planck's constant divided by 2π.

m is the electron mass.

v is the projectile velocity.

$\omega_o = \left(\frac{4\pi e^2 n_\varepsilon}{m}\right)^{\frac{1}{2}}$ is called the electron resonance frequency of the degenerate electron gas.

n_ε is the electron density in the electron gas.

Substitution of the known values of the constants into equation I-10 gives the relative electronic straggling as:

$$\frac{\Omega_\varepsilon^2}{\Delta E} \simeq 3.2 \times 10^{-16}\ n_\varepsilon^{1/4} \qquad \text{I-11}$$

where both Ω_ε and ΔE are expressed in keV.

Although nuclear straggling estimates have not been considered, comparisons can be made between equation I-11 and those of our experimental results in which nuclear collisions do not play a large role in the stopping process.

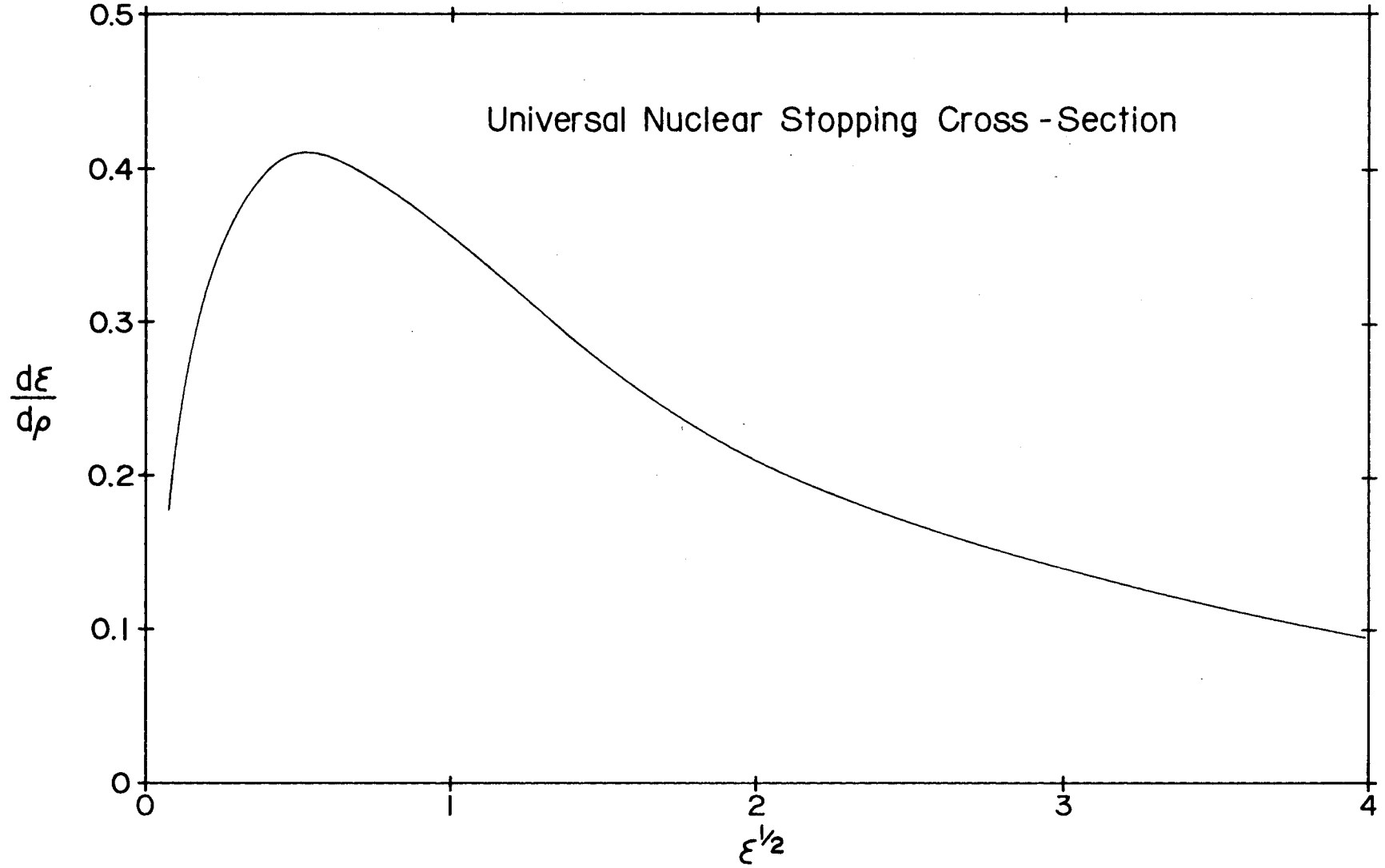
Universal Nuclear Stopping Cross-Section
0.5
0.4
0.3
0.2
0.1
0
dε/dρ
0
1
2
3
4
ε^1/2

FIG. 1

CHAPTER II

APPARATUS AND DATA ANALYSIS

1. Apparatus

The apparatus used in these experiments is shown schematically in Fig. 2. This apparatus has been described previously in references (W-62) and (O-63). The working pressure throughout the system was 3×10^{-6} torr.

Various ion sources were available to be used with the spectrometer. Alkali ions were obtained from a single filament surface ionization source. All other ions were obtained by the electron bombardment of a suitable vapour. Those substances that were not gaseous at room temperature were vapourized in an oven in the source.

The ions were accelerated to the required energy by a Brandenburg High Voltage Generator, Type MR100 R/1. The high voltage was continuously variable from 10-70 kilovolts.

The desired ions were selected in a ten inch, 90° magnetic spectrometer. Situated near the focus of the spectrometer was the thin boron film in which the ions lost energy. In front of the film were a pair of .020" slits which served to collimate the beam. The dimensions of the illuminated portion of the film were 0.7 cm x 0.5 mm. The film was mounted on a bellows assembly that allowed the film to be moved in and out of the path of the beam. During the course of an experiment the film was bombarded with approximately 10^{11} ions.

The energy of the emerging ions was determined in a seven inch, 90° electrostatic analyzer. Two such analyzers were available. One was fixed in the forward direction with an acceptance angle of 1.2°, and this was used in most of the experiments to be described. The other analyzer was mounted on a bellows arrangement so that the ions deflected by an angle (θ) from the forward direction could be analyzed. Again the acceptance angle was 1.2° and the limit of θ was ±13°. This analyzer was used to obtain experimental energy spectra in other than the forward direction in order to make comparisons with the spectra obtained from the Monte Carlo calculation.

Both electrostatic analyzers were designed in such a manner that the voltage across the plates multiplied by the number of charges carried by the ion was equal to one-tenth of the ion energy. The voltages for the analyzer plates were supplied by two Model 408A, Fluke power supplies, each with a calibration accuracy better than 0.25%.

The angular distribution of the ions emerging from the film was determined in a collimator which was mounted on a bellows. With this apparatus, ions of all energies were detected that had been deflected through the same angle, after suffering multiple collisions in passing through the film. At each angular setting (θ), the number of ions per unit solid angle ($N(\theta)\, d\Omega$) was determined. The limit of θ was ±17° from the forward direction.

With both electrostatic analyzers and with the collimator, the ions were detected in a 14 stage electron multiplier operated at 340 volts per stage. The output from the multiplier was amplified, and each event was recorded on a scaler.

2. Experimental Procedure and Data Analysis

The magnetic spectrometer was used to select the ion incident upon the film. Using one of the electrostatic analyzers, the energy spectrum of the ions emerging from the film was found by measuring the ion counting-rate at each energy setting. Two such energy spectra are shown in Fig. 3. The incident energy (E_{in}) was determined with the electrostatic analyzer after the film had been removed from the beam.

From each energy spectrum, the following energies were determined:

E_{out} = the most probable energy of the ions emerging from the film

$\Delta E = E_{in} - E_{out}$ = the most probable energy loss

$\bar{E} = \frac{1}{2}(E_{in} + E_{out})$

Two different methods were used to define E_{out}. When the energy spectrum was symmetric, as shown in Fig. 3a for the case of hydrogen stopping in boron, E_{out} was taken as the mid-point of the curve at half-height. For asymmetric spectra such as that for Ne^{20} stopping in boron shown in Fig. 3b, the points were joined to form a smooth curve. The peak of the asymmetric curve was taken as E_{out}.

The observed stopping cross-section S_o is defined at energy $\bar{E}$ by the following expression:

$$S_o = -\frac{1}{N}\frac{\Delta E}{t}$$

where $N = 1.30 \times 10^{23}$ atom/cm^3 for boron

t = film thickness

The work of Van Wijngaarden (W-62) showed that $\frac{\Delta E}{t}$ was independent of film thickness for films of thickness $\sim$ 100 - 500 Å. Thus S_o, as defined, is a property of the projectile-film material combination but is independent of the film thickness.

With a particular ion, S_o was determined over as wide an energy range as was practicable. For singly charged ions this was from 10 - 70 keV. When doubly charged ions were available, the energy range was extended to 140 keV.

For the lightest projectiles, the nuclear stopping cross-section calculated from Fig. 1 is relatively small at the energies used. The symmetric energy spectra obtained with light projectiles (for example hydrogen in Fig. 3a) indicate that the energy loss to nuclear collisions is negligible for projectiles emerging in the forward direction. As a result, the observed stopping cross-section (S_o) is equivalent to the electronic stopping cross-section (S_ε) for the light projectiles.

For the heavier projectiles, the energy spectra consist of a distinct peak and a low energy tail. Energy spectra for neon projectiles stopping in the same boron film are shown in Fig. 4. The tail of the distribution behaves in the manner expected of the nuclear energy loss; that is, the tail is relatively lower in magnitude at the higher energy. The peak of the distribution is essentially determined by the electronic energy loss; however, there is surely a small contribution from the nuclear energy loss also. A Monte Carlo calculation, developed by Ormrod (O-63) was used to determine the nuclear energy loss associated with ΔE.

In this calculation, an incoming particle is allowed to suffer collisions until it has advanced in the forward direction a distance equal to the film thickness. At this point, the computer types out the angle of emergence, final energy, and total nuclear energy loss of the projectile.

In each collision, the relative angle of deflection (θ) was selected by the generation of a random number. Each angle did not have an equal opportunity of selection, but each was weighted by the differential cross-section of Lindhard (L-63). The nuclear energy loss in the collision was given by equation I-2.

The electronic energy loss was approximated by assuming it to be given by a constant multiplied by the path length. The constant was adjusted to its best value after the calculation was complete, by sliding the energy scale of the calculated distribution to match best the experimental distribution. This procedure was justified because the total nuclear energy loss was the only important quantity determined from the calculation.

Calculations were performed with 25 keV and 40 keV neon ions passing through a 166 Å boron film.

The results of the calculation were first checked with the angular distribution measurements of all ions leaving the film. Comparison between calculation and experiment for 25 keV and 40 keV neon projectiles are shown in Fig. 5 and Fig. 6. The experimental values of $N(\theta)\, d\Omega$ are shown as the smooth curves. The calculated points were determined as $N(\theta)\, d\theta$ and the points shown in the figure have been divided

by sin θ in order to compare with experiment. The normalization of the experimental curves and experimental points was done by eye to give the best fit. The good agreement between the calculated and experimental points, gives us confidence that the calculation does give a valid simulation to the multiple collisions which a particle undergoes in passing through the film.

The calculated energy spectra were matched with experiment at angles of emergence of .075 , .025 , .175 , and .225 . Matchings with 25 keV neon projectiles are shown in Fig. 7. The calculated histograms and experimental curves were normalized to equal areas. At each of the angles of emergence, the calculation reproduced the general shape of the experimental curve. The decrease in energy of the peak at larger angles of emergence was also reproduced by the calculation.

The matching at each angle consisted of sliding the calculated results along the energy scale to reproduce best the experimental peak. The four independent positions were averaged to obtain the final position of the calculation on the energy scale. Finally, the total nuclear energy loss at the peak of the distribution was determined for particles emerging in the forward direction. The error in this nuclear energy loss was taken as that energy corresponding to the average difference from the mean of the four matchings.

When the total nuclear energy loss $\Sigma \Delta T_\nu$ was determined for projectiles emerging in the forward direction, then an effective nuclear stopping cross-section in the forward direction (S_ν^*) could be calculated from:

$$S_\gamma^* = -\frac{1}{Nt}\ \Sigma\Delta T_\gamma \qquad \text{II-1}$$

The electronic stopping cross section could then be calculated for the heavier projectiles by

$$S_\varepsilon = S_o - S_\gamma^* \qquad \text{II-2}$$

Calculations were performed with neon projectiles only. The results of these calculations were extended to other ions by using the universal nuclear stopping cross-section of Lindhard et al (L-63) shown in Fig. 1. At constant $\varepsilon^{\frac{1}{2}}$, the nuclear stopping in boron for atom B can be related to that for atom A by the following relation:

$$S_{\gamma B} = \frac{a_B\ Z_B\ (M_A + 10.82)}{a_A\ Z_A\ (M_B + 10.82)}\ S_{\gamma A} \qquad \text{II-3}$$

This result follows directly from the definition of the reduced stopping power $\frac{d\varepsilon}{d\rho}$ given in equation I-6.

At constant ε the differential scattering cross-section for atom A and atom B are identical (L-63). Hence, the ratio of S_γ^* to S_γ is the same for both atom A and atom B, and equation II-3 can be written as

$$S_{\gamma B}^* = \frac{a_B\ Z_B\ (M_A + 10.82)}{a_A\ Z_A\ (M_B + 10.82)}\ S_{\gamma A}^* \qquad \text{II-4}$$

One can use the calculated value of S_γ^* for neon projectiles, along with equation II-4, to calculate S_γ^* for all of the other projectiles. The electronic stopping cross-section for all the projectiles can then be determined from the observed stopping cross-section and equation II-2.

The energy dependence of the electronic stopping cross-section was taken to be of the form

$$S_\varepsilon = kE^P \qquad \text{II-5}$$

The justification for equation II-5 was twofold:

1) Such a form was exhibited by ions requiring no correction, both in the present work and in the work of Ormrod (O-63) and (O-64).

2) The theory of Lindhard et al (L-63) predicts such a form with $P = 0.5$.

Since the nuclear stopping diminishes at higher energies, S_ε must approach S_o in this region. Thus, on a plot of log S versus log E, S_ε was represented by the best straight line through the Monte Carlo points which approached S_o asymptotically at high energy.

APPARATUS

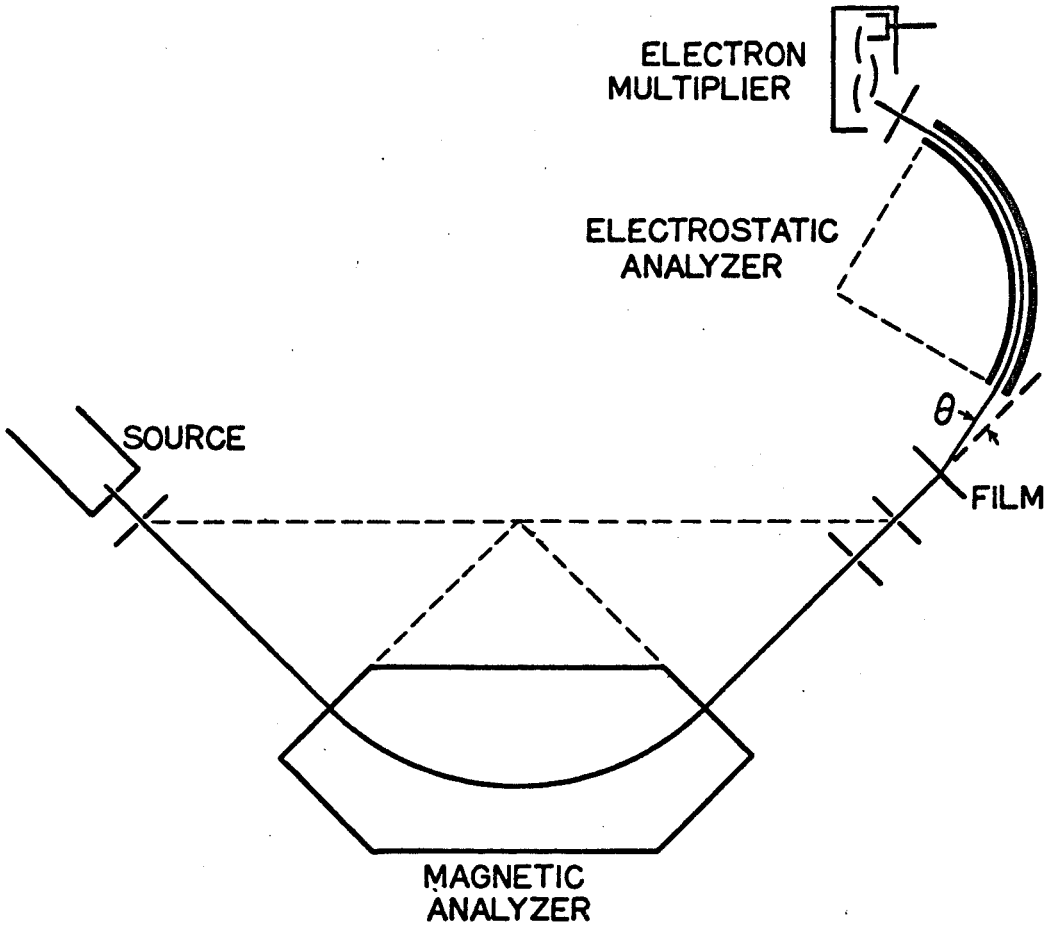

FIG. 2

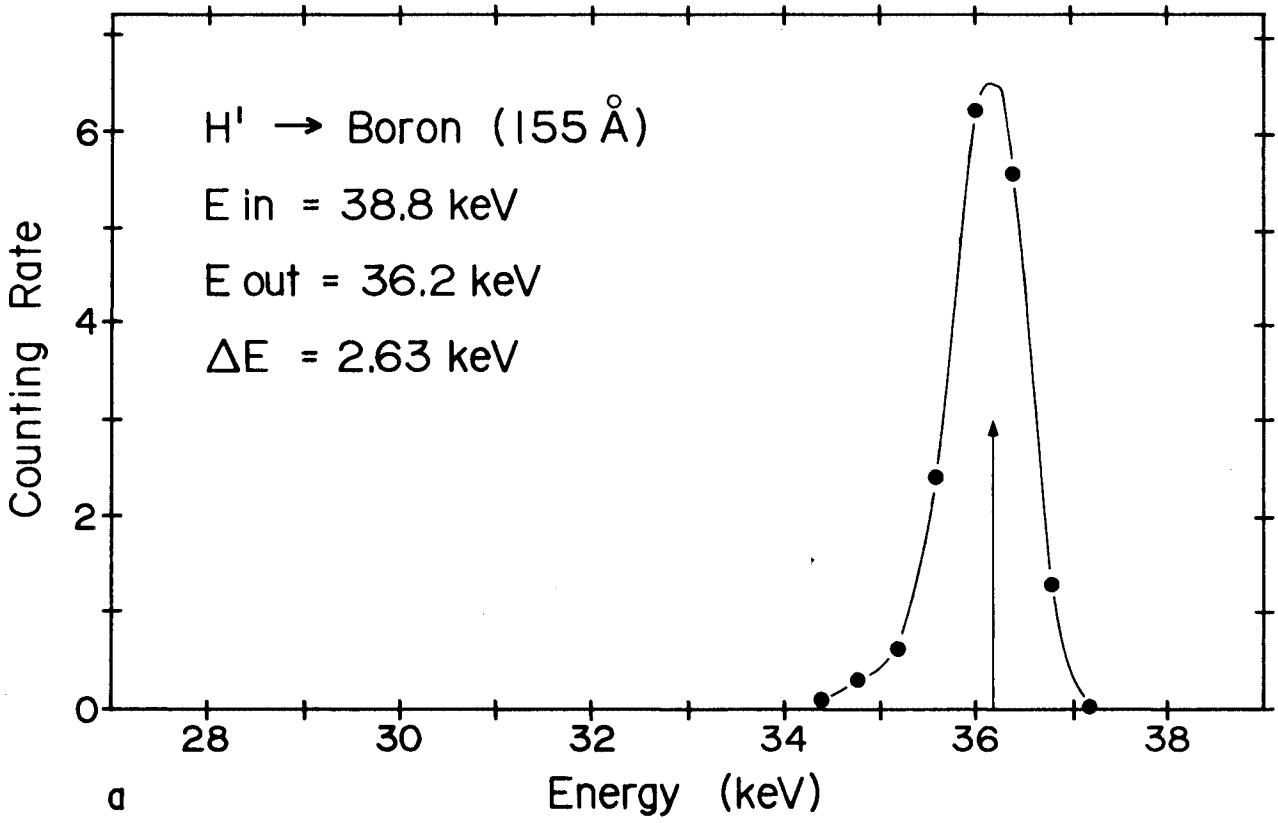
H' → Boron (155 Å)
E in = 38.8 keV
E out = 36.2 keV
ΔE = 2.63 keV
Counting Rate
0
2
4
6
28
30
32
34
36
38
Energy (keV)
a

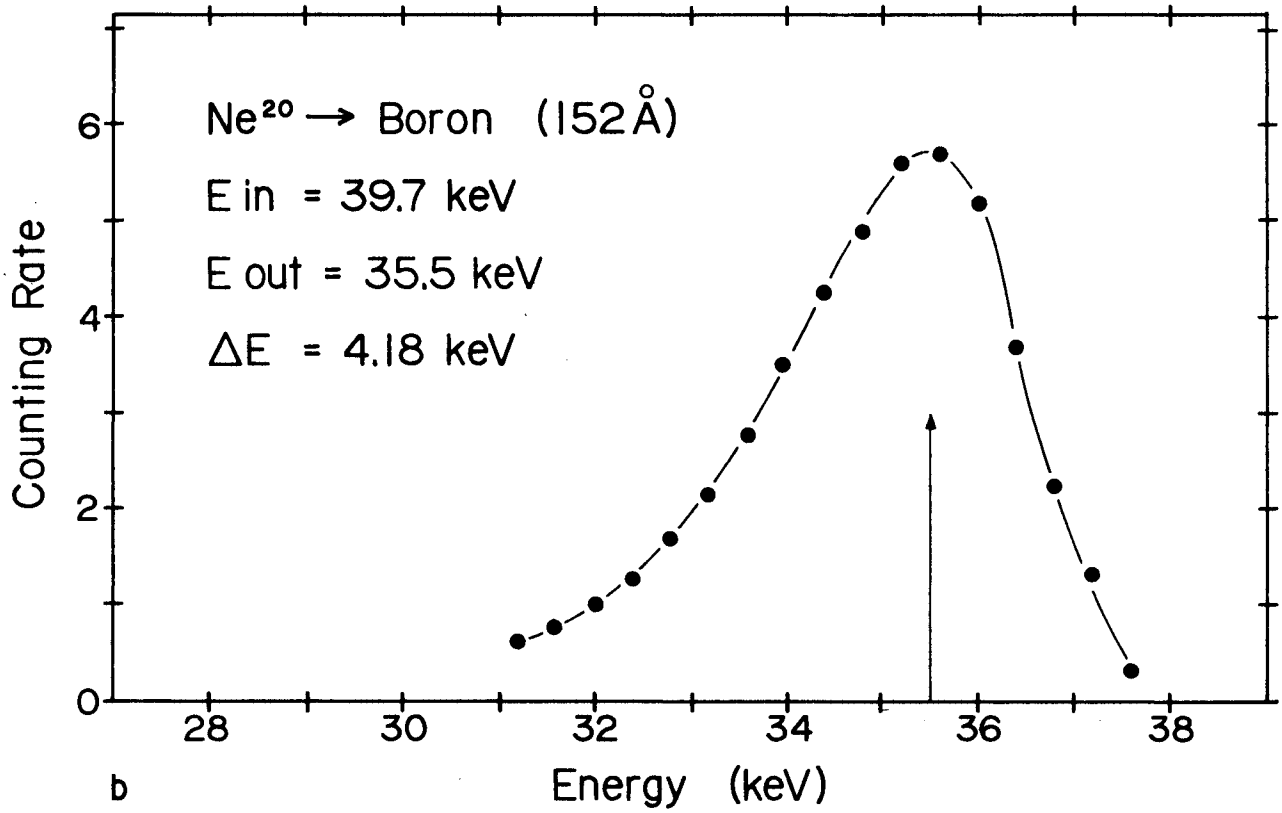
Ne²⁰ → Boron (152 Å)
E in = 39.7 keV
E out = 35.5 keV
ΔE = 4.18 keV
Counting Rate
0
2
4
6
28
30
32
34
36
38
Energy (keV)
b

FIG. 3

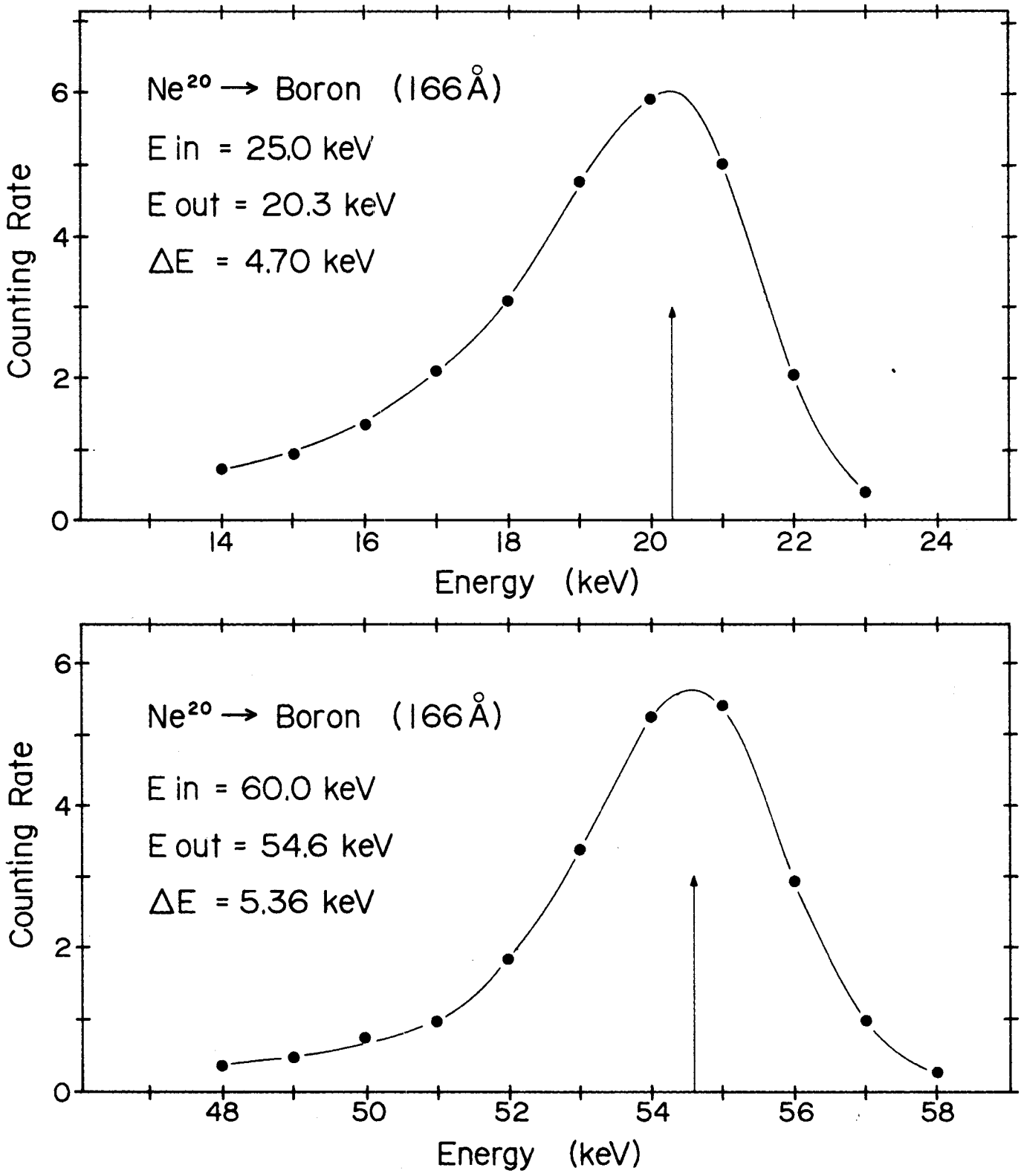
Ne²⁰ → Boron (166 Å)
E in = 25.0 keV
E out = 20.3 keV
ΔE = 4.70 keV
Counting Rate
Energy (keV)
Ne²⁰ → Boron (166 Å)
E in = 60.0 keV
E out = 54.6 keV
ΔE = 5.36 keV
Counting Rate
Energy (keV)

FIG. 4

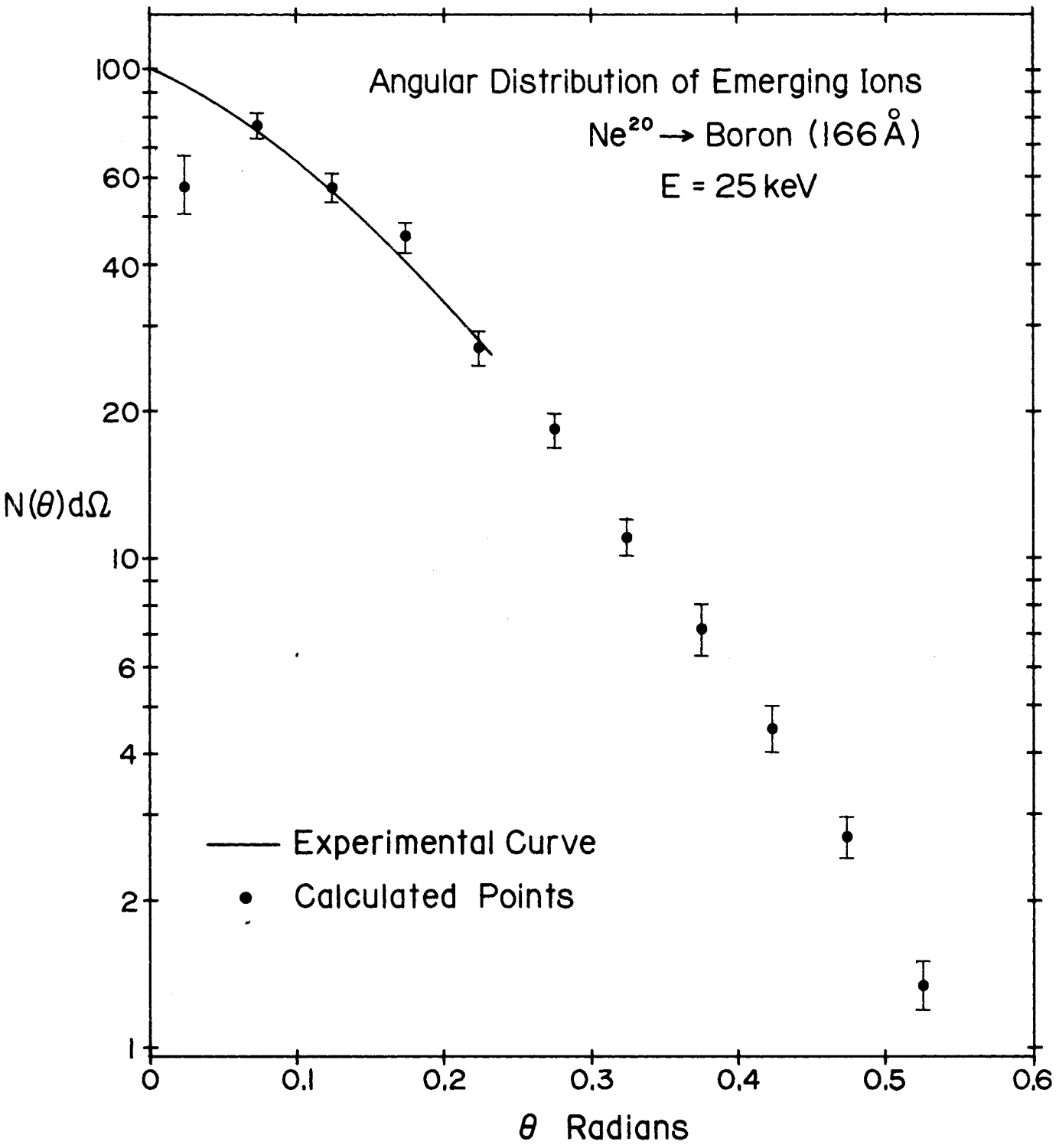
Angular Distribution of Emerging Ions
Ne20 → Boron (166 Å)
E = 25 keV
100
60
40
20
10
6
4
2
1
N(θ)dΩ
Experimental Curve
Calculated Points
0
0.1
0.2
0.3
0.4
0.5
0.6
θ Radians

FIG. 5

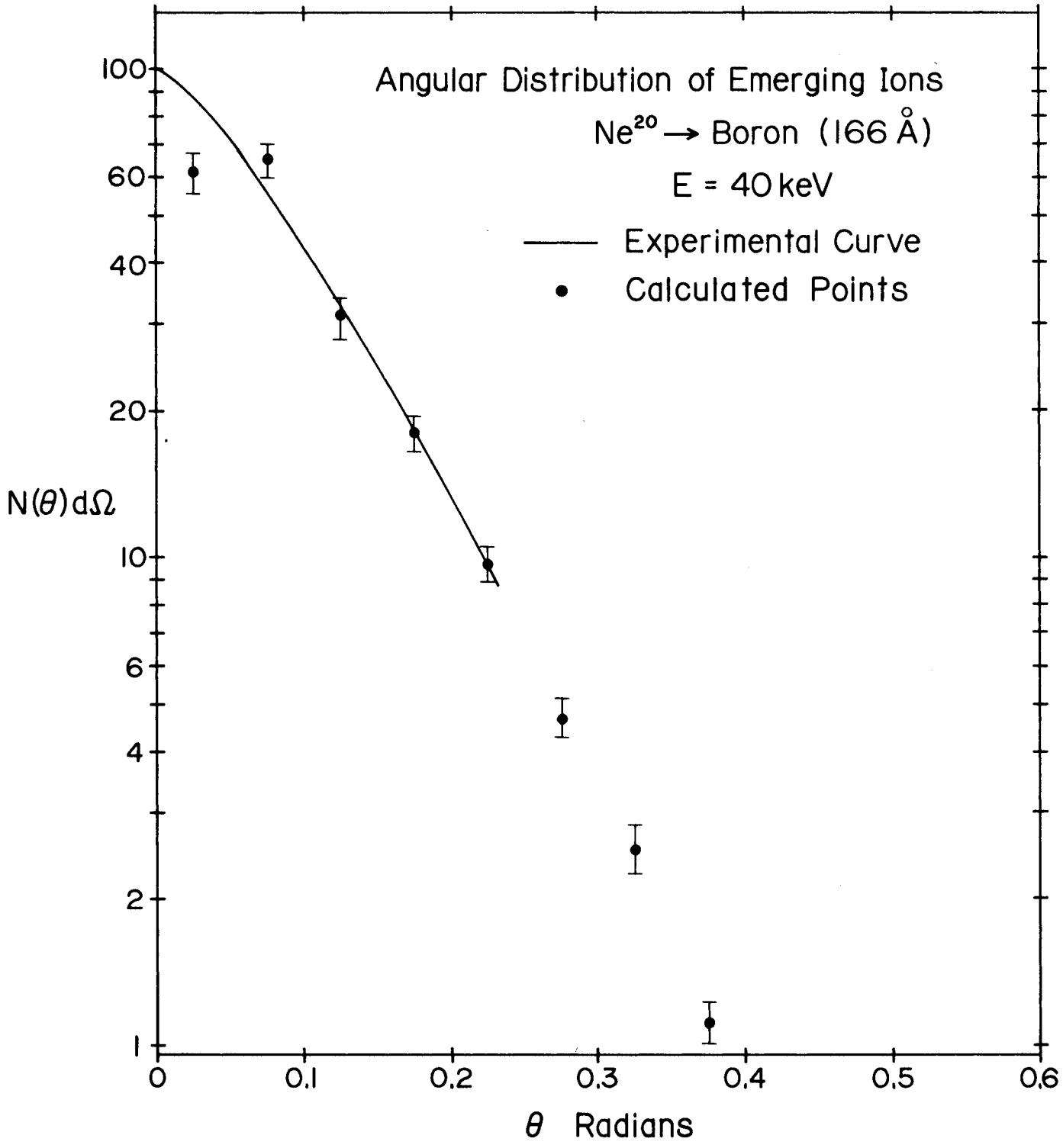
Angular Distribution of Emerging Ions
Ne20 → Boron (166 Å)
E = 40 keV
Experimental Curve
Calculated Points
N(θ) dΩ
100
60
40
20
10
6
4
2
1
0
0.1
0.2
0.3
0.4
0.5
0.6
θ Radians

FIG. 6

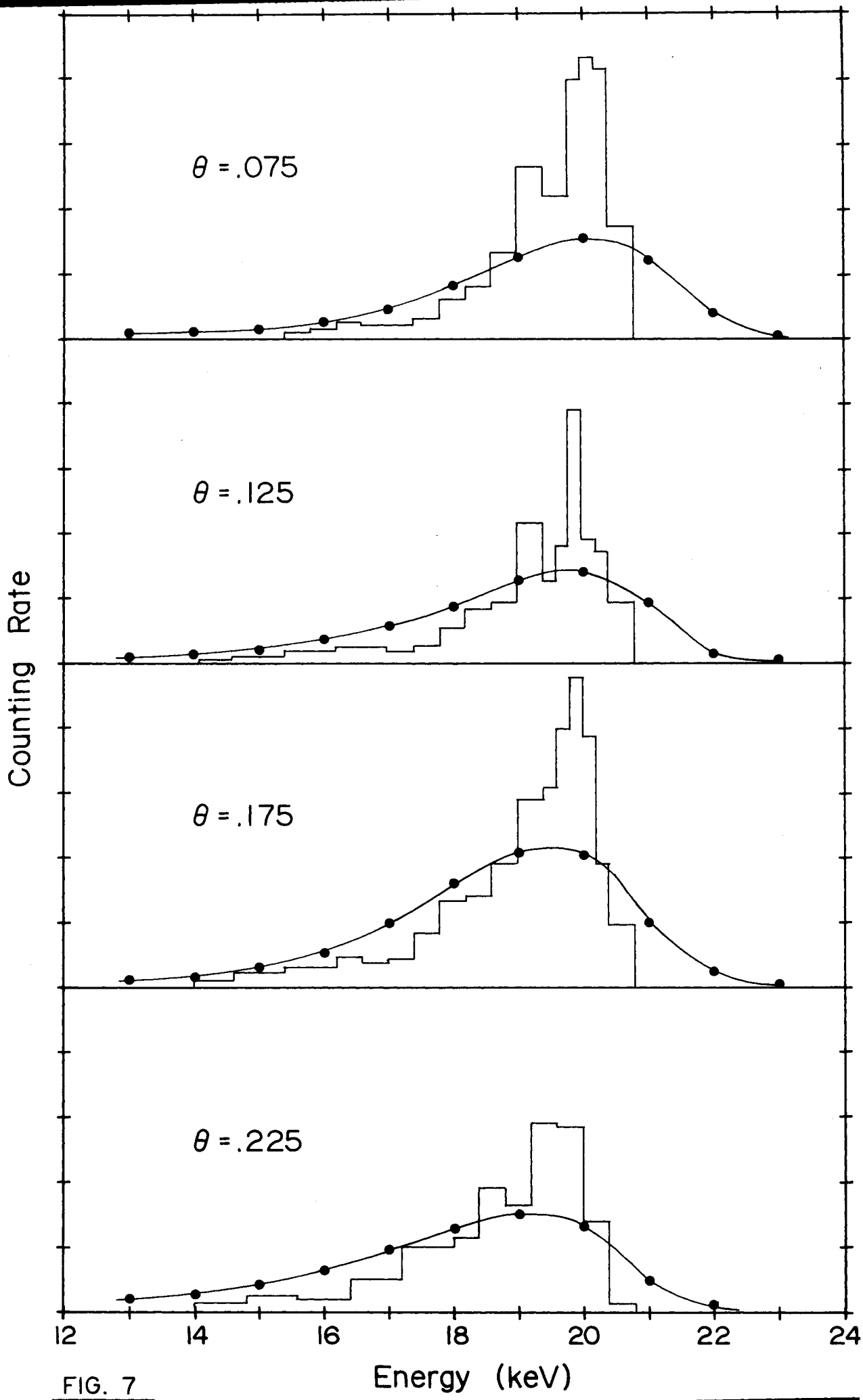
θ = .075
θ = .125
θ = .175
θ = .225
Counting Rate
12
14
16
18
20
22
24
Energy (keV)

FIG. 7

CHAPTER III

THIN FILMS

1. Production of the Films

The targets used in these experiments were boron films ranging from 80 Å to 1600 Å in thickness. The films were made by vacuum-depositing boron onto clean microscope slides in a specially-constructed coating unit. The films were stripped from a slide by allowing distilled water to rise slowly over the slide while it was held in a tray at an angle of $\sim 10°$. To facilitate stripping, some of the films were deposited on a substrate of barium chloride on the glass slides, following the technique of Woytowich and described by Yaffe (Y-63). During stripping, the barium chloride dissolved and the films floated free. Subsequent experiments with these films gave results identical to those from experiments with the films deposited without $BaCl_2$ substrate. The films were picked up on a nickel mesh with 1000 lines per inch allowing 49% transmission. The mesh was obtained commercially from the Buckbee-Mears Co. of St. Paul, Minnesota.

The boron was evaporated using a modification of an electron bombardment technique suggested by the work of Muggleton (M-61) and Adair (A-62). A photograph of the apparatus is shown in Fig. 8. A tungsten ribbon filament surrounds the boron which is in the form of a pellet. The pellet is 3/8" long and is supported on a horizontal copper plate attached to 1/4" o.d. copper tubing. The tubing passes out of the

vacuum system through insulated sleeves and then is connected to a cold water system through 12" lengths of rubber hose, which provide a high electrical resistance from the copper tubing to ground.

The heated filament is held at ground potential, and the water cooled copper tube and boron pellet are at a positive potential variable up to 800 volts. With an emission current of $\sim$170 ma at $\sim$500 volts, the tip of the boron pellet became molten and could be kept molten by gradually increasing the filament temperature and the anode voltage.

The glass slides were held in a brass holder about 9 cm above the boron pellet. During evaporation, a magnetically controlled shield was held between the boron pellet and the glass slides until the pressure in the system had fallen to 5×10^{-6} torr. Prior to the removal of the shield, the system was flushed with helium as described by Strivastava (S-61). The deposition time ranged from $\sim$ 20 seconds for the thinnest to several minutes for the thickest films.

2. Thickness of the Boron Films

The thickness of the boron films was determined by observing the energy loss of protons passing through the film. This method was calibrated by determining the stopping cross-section of 30 keV protons in thick weighed films. Each thick film was mounted without backing on a nickel holder. After the proton energy loss had been determined, the film was cut out of the holder and weighed on a microbalance (Mettler Micro Gram-atic). The thickness of the film was determined by assuming that the density of the boron film was 2.34 g/cm^3, the same as the bulk density of boron.

The energy loss at 30 keV was calculated by determining the energy loss at an incident energy above 30 keV. Then the result was normalized to 30 keV by approximating the proton energy loss curve of Fig. 13 by the following relation:

$$-\frac{\Delta E}{\Delta x} = a E^{P_1} \quad \text{for } 20 < E \leq 30 \text{ keV}$$

$$-\frac{\Delta E}{\Delta x} = b E^{P_2} \quad \text{for } 30 \leq E < 40 \text{ keV} \qquad \text{III-1}$$

The film thickness could be expressed in terms of the parameters a, b, P_1 and P_2 by substituting equation III-1 into

$$t = \int_{E_{out}}^{E_{in}} \left(-\frac{\Delta E}{\Delta x}\right)^{-1} dE \qquad \text{III-2}$$

The energy loss at an average energy loss could be given in terms of the parameters a/b, P_1, and P_2 from the following relation:

$$\Delta E_{30} = a E^{P_1} t \qquad \text{III-3}$$

The parameters were determined from experiments with four thin films. The results were used to obtain the following empirical equation:

$$\Delta E_{30} = 3.38 E_{in}^{.73} - 5.61 E_{out}^{.63} + 7.01 \qquad \text{III-4}$$

For each thick film, several values of ΔE_{30} were calculated from experimental results at different incident energies. The agreement between the different determinations was very good, and the probable error in ΔE_{30} was found to be less than 1%.

Table III-1 summarizes the results of the calibration experiment. S_o is the observed stopping cross-section of 30 keV protons in boron.

A probable error of ± 2μg was estimated in the weighing of each film. Percentage probable errors of 2% and 1% were estimated in the area of the weighed film and in the determination of ΔE_{30} respectively. Then the percentage probable error in each value of S_o was calculated by the following method:

$$\text{P.P.E. in } S_o = \left[\left(\frac{200}{W}\right)^2 + (2)^2 + (1)^2\right]^{1/2} \qquad \text{III-5}$$

where W is the weight of the film in μg.

From the values of S_o in Table III-1, a weighted mean was calculated to be

$$S_o = 1.23 \times 10^{-14} \text{ eV - cm}^2\text{/atom} \pm 3.6\%.$$

The quoted error is the percentage probable error in the weighted mean.

The thickness of thin boron films was determined from the following relation:

$$t = \frac{\Delta E}{.01598} \text{ Å} \pm 3.6\%$$

where ΔE is the energy loss in keV of 30 keV protons stopping in boron.

TABLE III-1

The Determination of the Absolute Stopping Cross-Section for 30 keV Protons in Boron

Weight (μg)	Surface Density ($\mu g/cm^2$)	Thickness (Å)	ΔE_{30} (keV)	$S_o \times 10^{14}$ ($eV\text{-}cm^2/atom$)	P.P.E. in S_o (%)
15	21.7	930	14.89	1.232	13.5
19	28.1	1201	19.52	1.247	10.7
20	28.1	1201	19.65	1.256	10.2
35	33.0	1410	22.68	1.235	6.1
36	34.3	1465	23.08	1.210	6.0

3. Quality of the Boron Films

The 9 cm distance between the microscope slides and the molten boron, introduced a 10% variation in source to slide distance from the edge to the middle of a slide. A corresponding variation in film thickness would be expected across the slide. The ion beam dimension was 0.7 cm x 0.5 mm and the maximum variation in thickness over the illuminated portion of the film was $\sim$ 2%. However, this variation could be reduced further by orientating the film on the holder so that the long dimension of the illuminated portion of the film was approximately the same distance from the source during deposition.

The shape of the energy spectrum of 30 keV protons was used as the criterion by which to judge the acceptability of a given film. Any asymmetry to the spectrum shape of Fig. 3a was attributed to variations in thickness across the film. Such films were discarded.

Local irregularities in the film surface could be caused by the surface of the glass substrate. Examination of films in an electron microscope, revealed few surface features attributable to the glass slide. A typical microscope photograph of a boron film with a total magnification of 42,000 is shown in Fig. 9. The most striking feature of the photograph is the lack of any pronounced surface structure.

The crystal structure of the films was studied by an examination of the electron diffraction patterns produced by the films. Fig. 10 is a photograph of the electron diffraction pattern of the film shown in Fig. 9. The diffuse, broad concentric rings of the diffraction pattern indicate that the film is amorphous (B-36). The only structure in the film is that associated with the nearest neighbour separation of the atoms making up the film.

For comparison, Figures 11 and 12 are included to show the surface features and significant crystal structure in an electroplated nickel film. Fig. 11 is a photograph with a total magnification of 45,000, and Fig. 12 is a diffraction pattern taken in the same region of the film.

The lack of structure in the bo... films made them particularly suitable for the experiments described in this thesis. An amorphous structure of the solid was assumed both in the Monte Carlo calculation, and in the theoretical treatment of the stopping process with which our experimental results were compared.

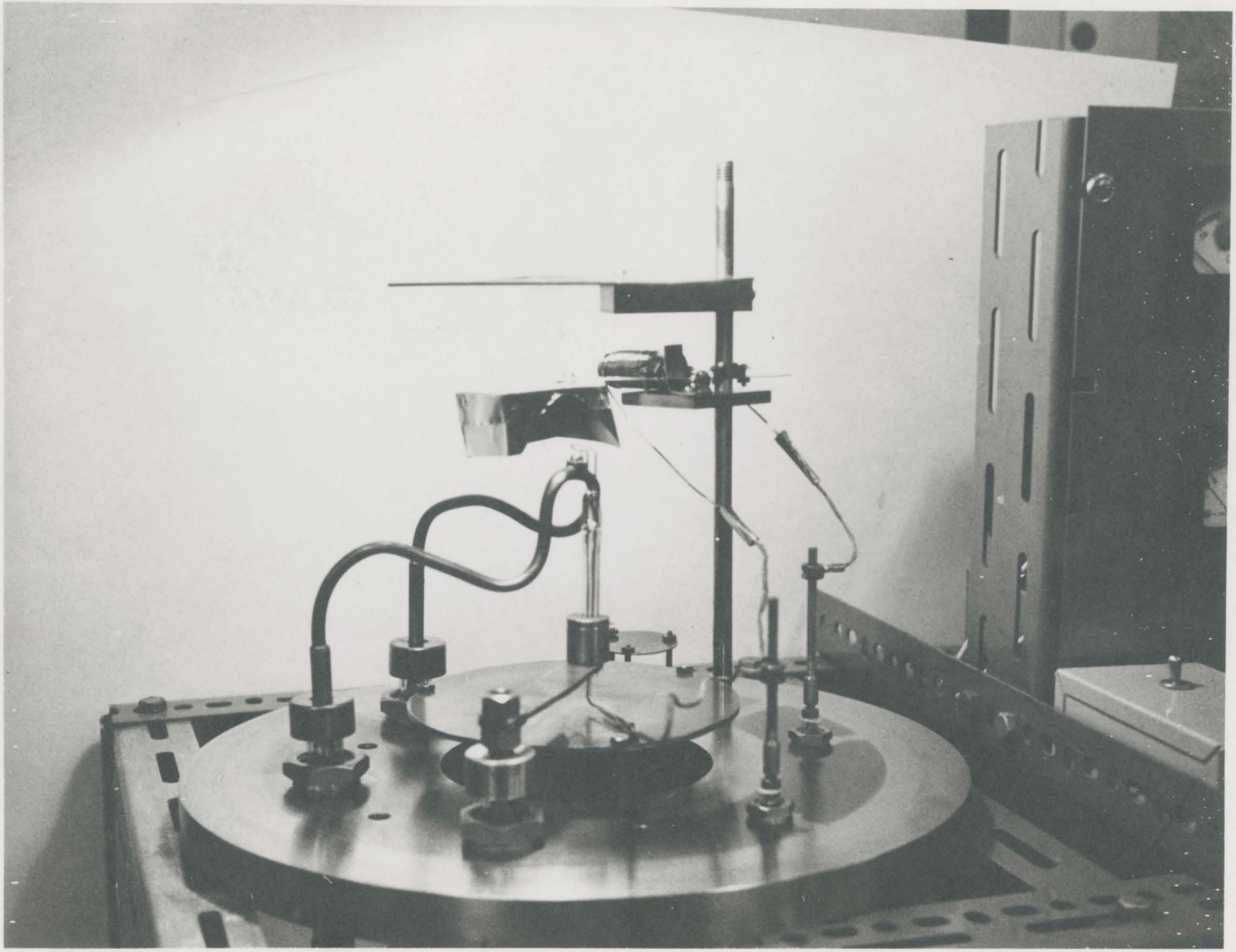

FIG. 8

FIG. 9

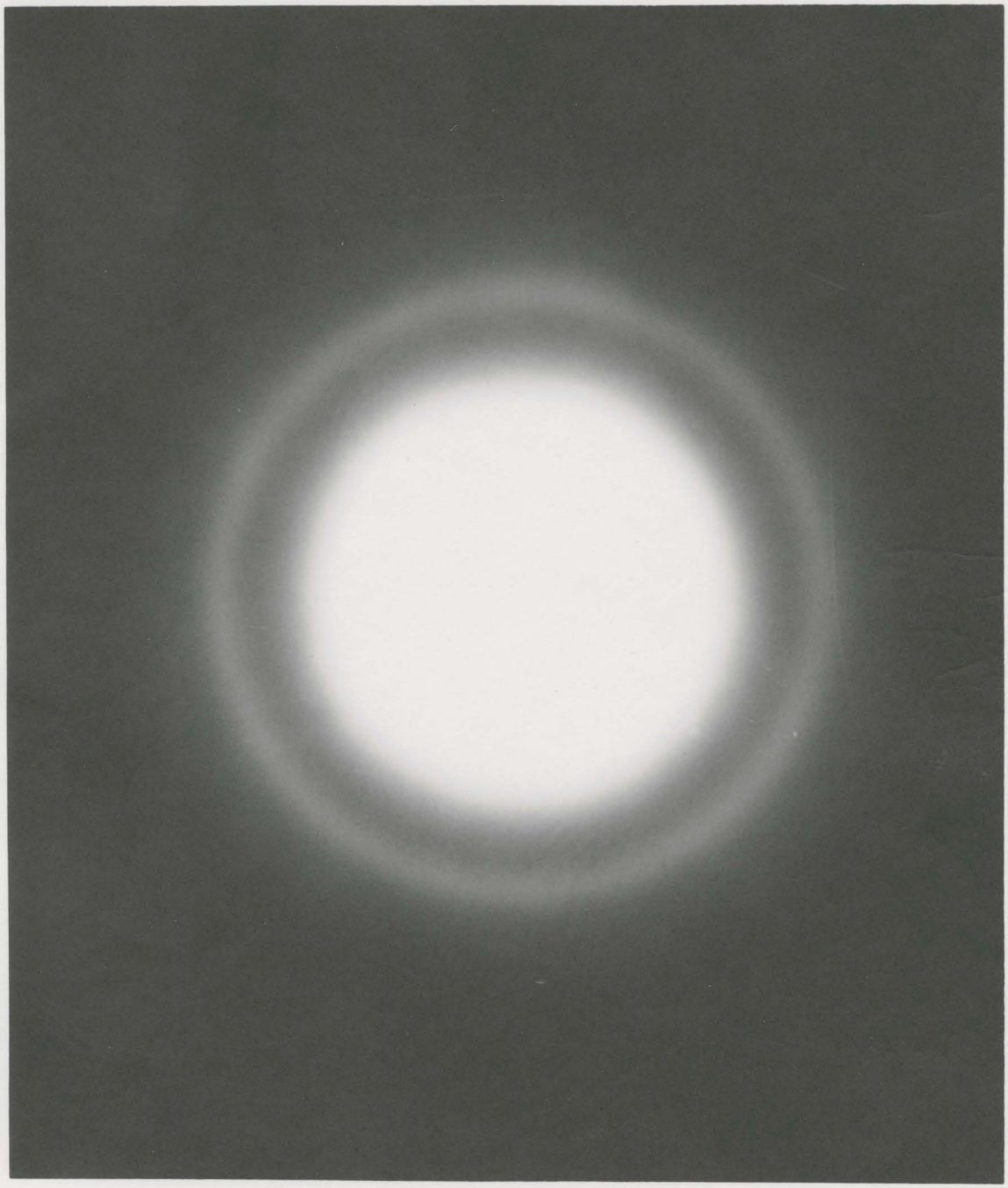

FIG. 10

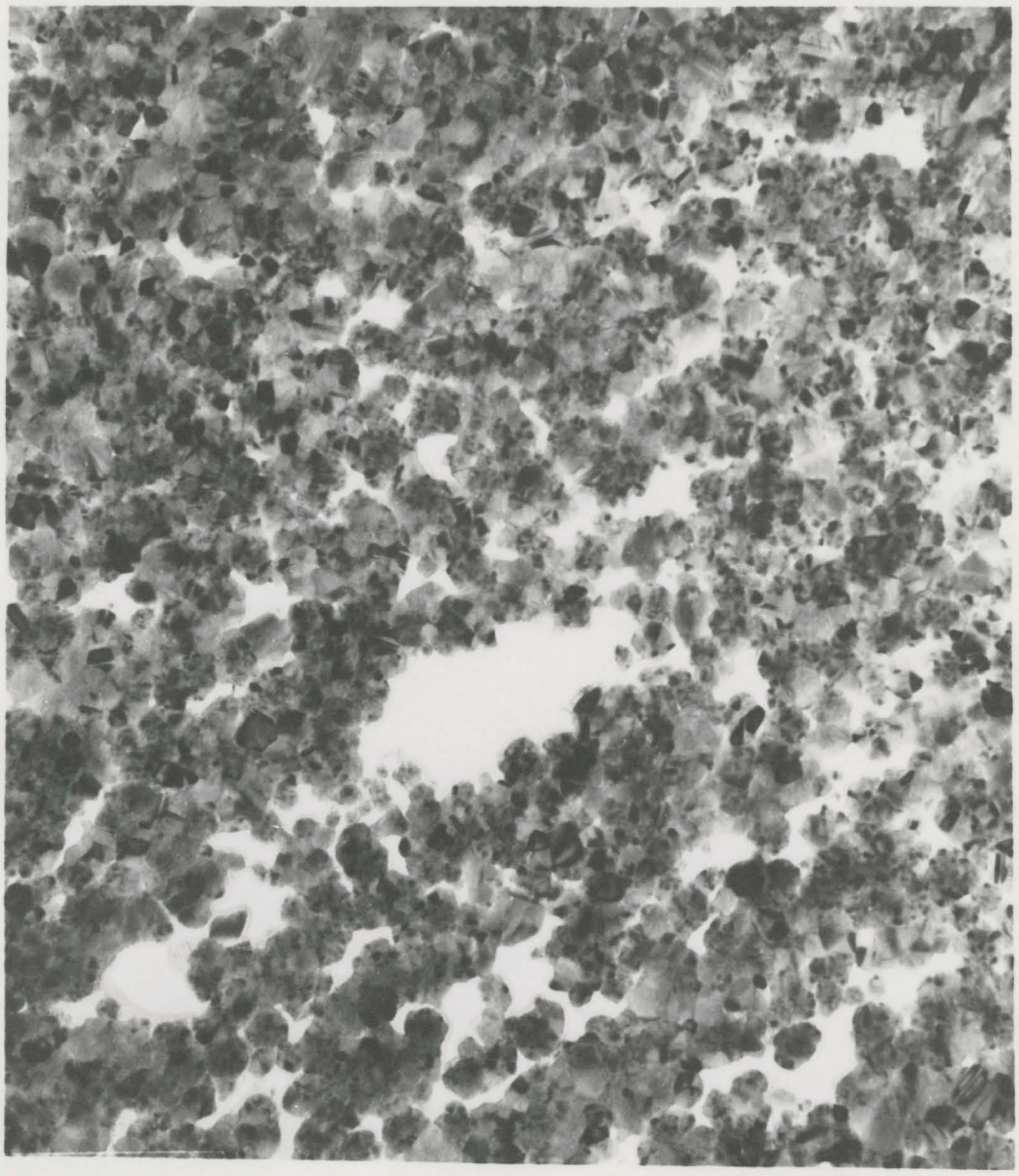

FIG. II

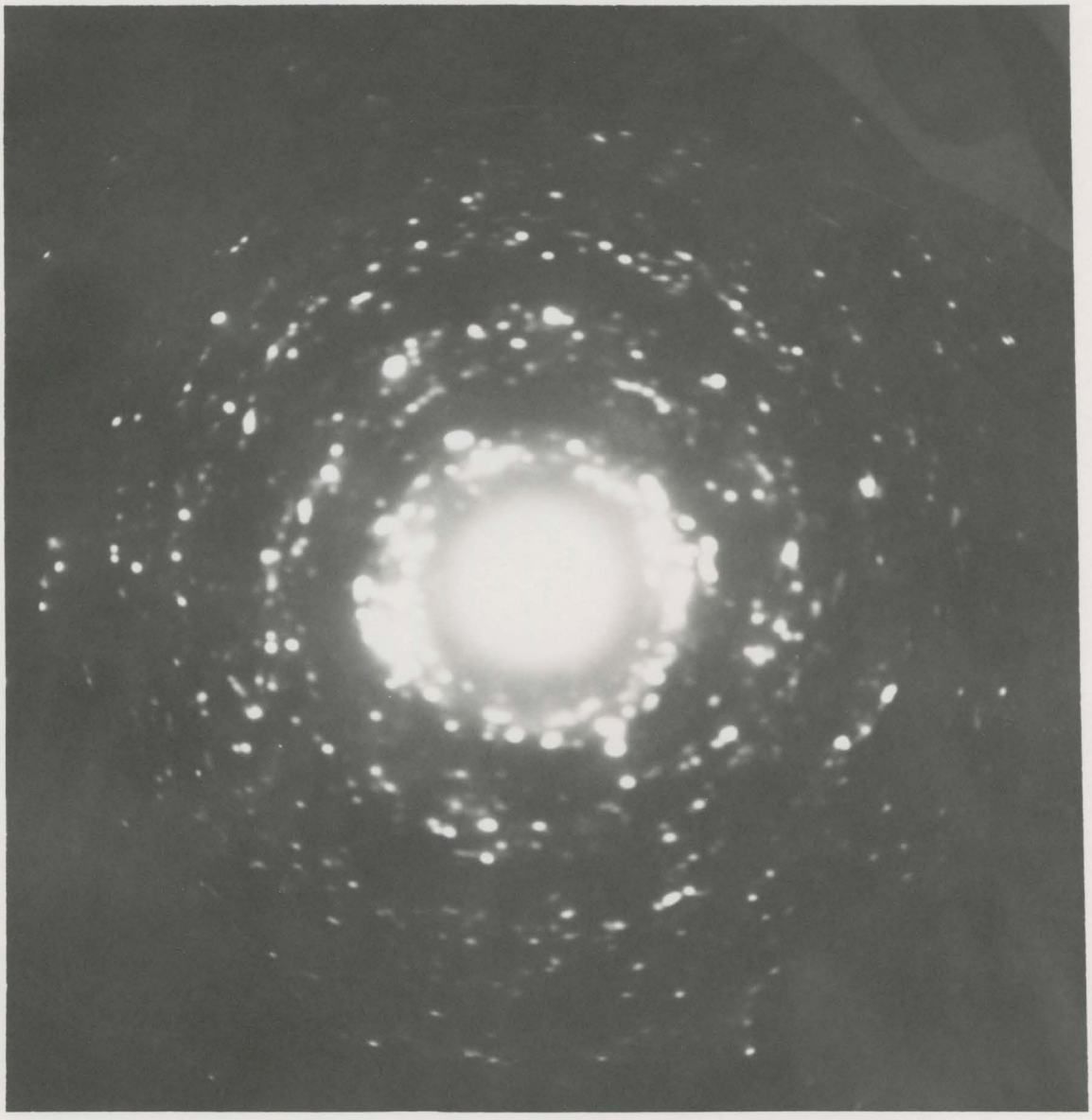

FIG. 12

CHAPTER IV

EXPERIMENTAL RESULTS

1. Stopping Cross-Sections

The observed stopping cross-sections for hydrogen are shown in Fig. 13. The results with protons are shown as the solid dots, while the deuteron results are shown as the open circles.

The hydrogen curve represents an absolute determination of S_o since some of the experiments were performed with weighed films, as described in section III-2.

The nuclear stopping cross-section determined from Fig. 1 is less than 1% of the observed stopping cross-section for hydrogen at 10 keV. Since S_ν^* is only a fraction of S_ν, the nuclear stopping is a negligible portion of S_o, and hence $S_o = S_\varepsilon$ for hydrogen. The probable error in S_ε was 4%.

In Figures 14 to 22 the nuclear stopping cross-section, S_ν, is shown along with the observed and electronic stopping cross-sections (S_o) and (S_ε) for each projectile stopping in boron. For each atom, S_ν is an explicit solution of the universal nuclear stopping cross-section shown in Fig. 1.

The stopping cross-sections for helium and lithium in boron are shown in Fig. 14 and Fig. 15. As determined by the extension of the Monte Carlo calculation, the nuclear contribution to S_o is negligible above 3 keV for helium and above 9 keV for lithium. As our experi-

mental energy range did not extend below 10 keV, the observed and electronic stopping cross-sections are equivalent for helium and lithium projectiles.

Although the contribution of nuclear stopping in the forward direction is negligible for helium and lithium, the total nuclear stopping cross-section for these projectiles is not. For helium projectiles incident on boron (denoted $He^4 \rightarrow$ Boron), S_ρ amounts to 6% of S_ε at 20 keV. For $Li^7 \rightarrow$ Boron, S_ρ amounts to 26% of S_ε at 20 keV.

The nuclear contribution to S_o was significant for all other projectiles and the results of the Monte Carlo calculation were used to calculate S_ε. Whenever the calculation was used, the probable error in S_ε was greater than the 4% error associated with S_o and the film thickness.

The stopping cross-sections for boron, carbon, nitrogen, oxygen, fluorine, neon, and sodium are shown in Figures 16 to 22. At the higher energies the probable errors in S_ε range from 4% where no correction was required, to 9% for sodium where a 12% correction was required. At the lower energies where the Monte Carlo corrections were larger, the probable error was somewhat greater.

The results of the Monte Carlo calculation with 25 keV and 40 keV neon projectiles are shown as crosses with error bars in Fig. 21. The electronic stopping cross-section was approximated by a straight line on the plot of log S versus log E through the two calculated points and approaching S_o asymptotically at higher energies. The asymptotic approach of S_ε to S_o was dictated by the decrease in the magnitude of nuclear stopping at higher energies.

This form of the electronic stopping cross-section was expressed in Chapter II by the following equation:

$$S_\varepsilon = kE^P \qquad \text{II-5}$$

The coefficients k and the exponents P for each projectile studied, along with the domain of applicability of equation II-5 for each, are given in Table IV-1.

The percentage probable error in the exponent P ranges from somewhat less than 2% for H^1 to about 6% for Na^{23}. These probable errors are less than the errors in S_ε because the absolute determination of film thickness was not required to determine the slopes (P) of the curves in Figures 13 to 22.

2. Straggling

The straggling in energy of hydrogen and helium projectiles passing through boron was determined from each experimental energy distribution. The half-width at half-height of the transmitted energy spectrum was called the observed straggling (Ω_o). A small correction to Ω_o was made to take into account the energy spread of the incident beam by assuming that

$$\Omega^2 = \Omega_o^2 - W^2 \qquad \text{IV-1}$$

where Ω is the "true" straggling caused by collision processes in the film.

$W = \frac{E}{350}$ is an empirical estimate approximating the width of the incident beam at energy E.

No correction was made for any component of Ω caused by slight variations in film thickness.

TABLE IV-1

Coefficients (k) and Exponents (P) for the Electronic Stopping Cross-Sections in Boron as Expressed in the Equation $S_\varepsilon = kE^P$

Atom	$k \times 10^{15}$ (eV-cm^2/atom)	P	Energy Domain (keV)
H^1	3.2	0.40	12-25
H^2	2.4	0.41	13-40
He^4	3.6	0.42	15-70
Li^7	2.4	0.47	15-70
B^{11}	3.2	0.51	15-140
C^{12}	4.9	0.47	15-140
N^{14}	4.5	0.49	15-140
O^{16}	4.7	0.47	15-140
F^{19}	4.1	0.46	15-140
Ne^{20}	2.9	0.51	20-140
Na^{23}	2.7	0.46	25-70

Any single determination of Ω was uncertain by $\sim 20\%$. However a technique was used by which more reliable results could be obtained. Van Wijngaarden and Duckworth (W-62) found that $\frac{\Omega}{\Delta E}$ was constant for the same film-projectile combination. A mean value of $\frac{\Omega}{\Delta E}$ was calculated from all experiments with hydrogen stopping in a given film. ΔE was determined experimentally at the required energy with a probable error estimated at 2%, and then the corresponding value of Ω was calculated. The percentage probable error in Ω was calculated in the following manner:

$$\text{P.P.E. in } \Omega = \left[\left(\text{P.P.E. in } \frac{\Omega}{\Delta E} \right)^2 + (2)^2 \right]^{1/2} \qquad \text{IV-2}$$

where the percentage probable error in $\frac{\Omega}{\Delta E}$ was determined from the distribution of individual $\frac{\Omega}{\Delta E}$ values. The P.P.E. in Ω ranged from 3% to 12%.

The straggling of hydrogen projectiles was determined at a particle velocity $v = v_o$. This is equivalent to a proton energy of 25 keV and a deuteron energy of 50 keV. The results are presented in Fig. 23, in which Ω^2 is plotted as a function of ΔE. The relative straggling of hydrogen in boron as determined from the slope of the best line drawn through the experimental points was

$$\frac{\Omega^2}{\Delta E} = 0.055 \text{ keV} \pm 5\% \text{ (at } v = v_o)$$

A plot of Ω^2 versus ΔE was not possible for results with helium projectiles because experiments were performed with two thin films only. With each film, $\Omega^2/\Delta E$ was calculated at a particle velocity of $0.5\ v_o$

from the values of $\frac{\Omega}{\Delta E}$ and ΔE determined in the manner discussed above. The result of the relative straggling of helium in boron was

$$\frac{\Omega^2}{\Delta E} = 0.054 \text{ keV} \pm 12\% \text{ (at } V = .5\ V_o)$$

Straggling determinations were not carried out with the heavier projectiles, because of the lower counting rates and asymmetric energy distributions encountered with these ions.

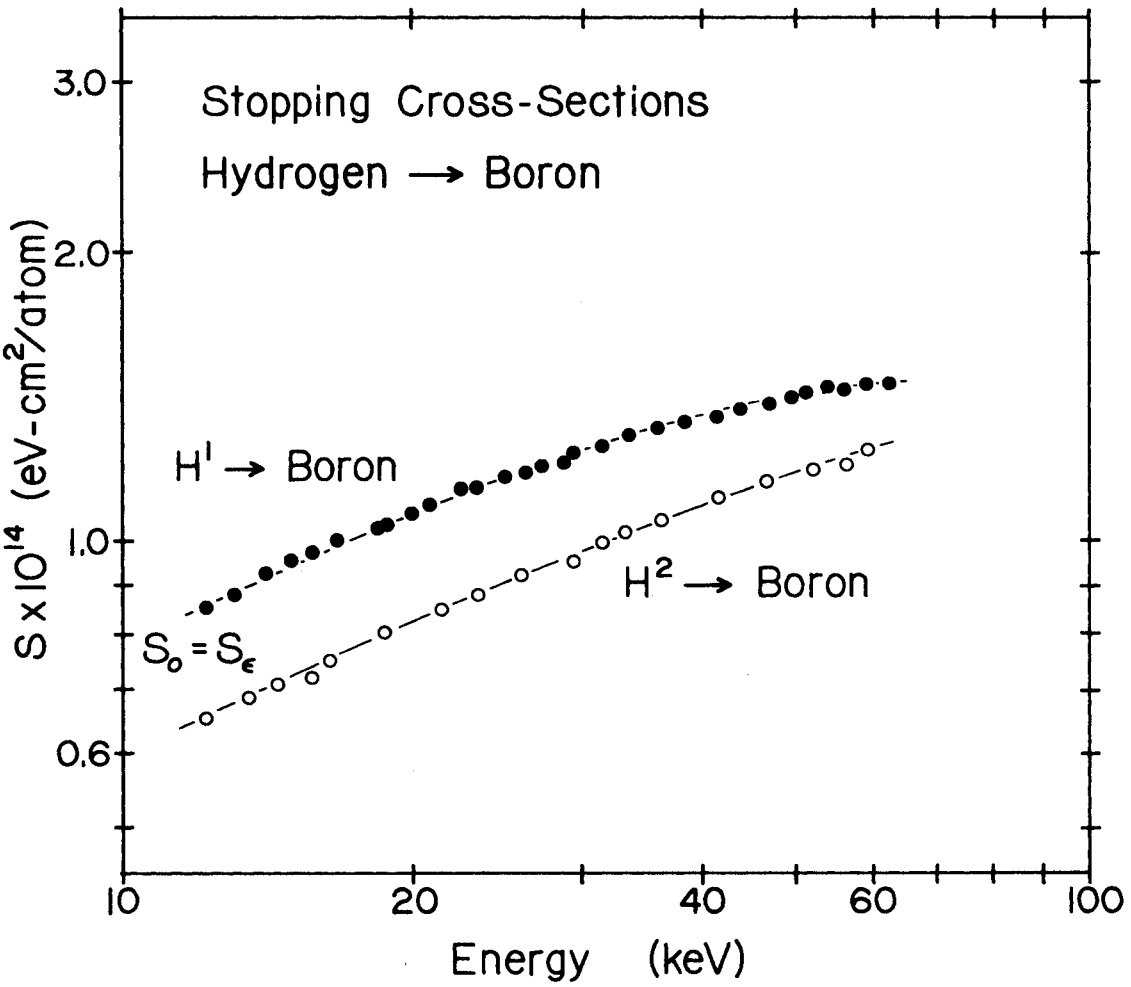
Stopping Cross-Sections
Hydrogen → Boron
H¹ → Boron
H² → Boron
S₀ = Sε
S x 10¹⁴ (eV-cm²/atom)
3.0
2.0
1.0
0.6
10
20
40
60
100
Energy (keV)

FIG. 13

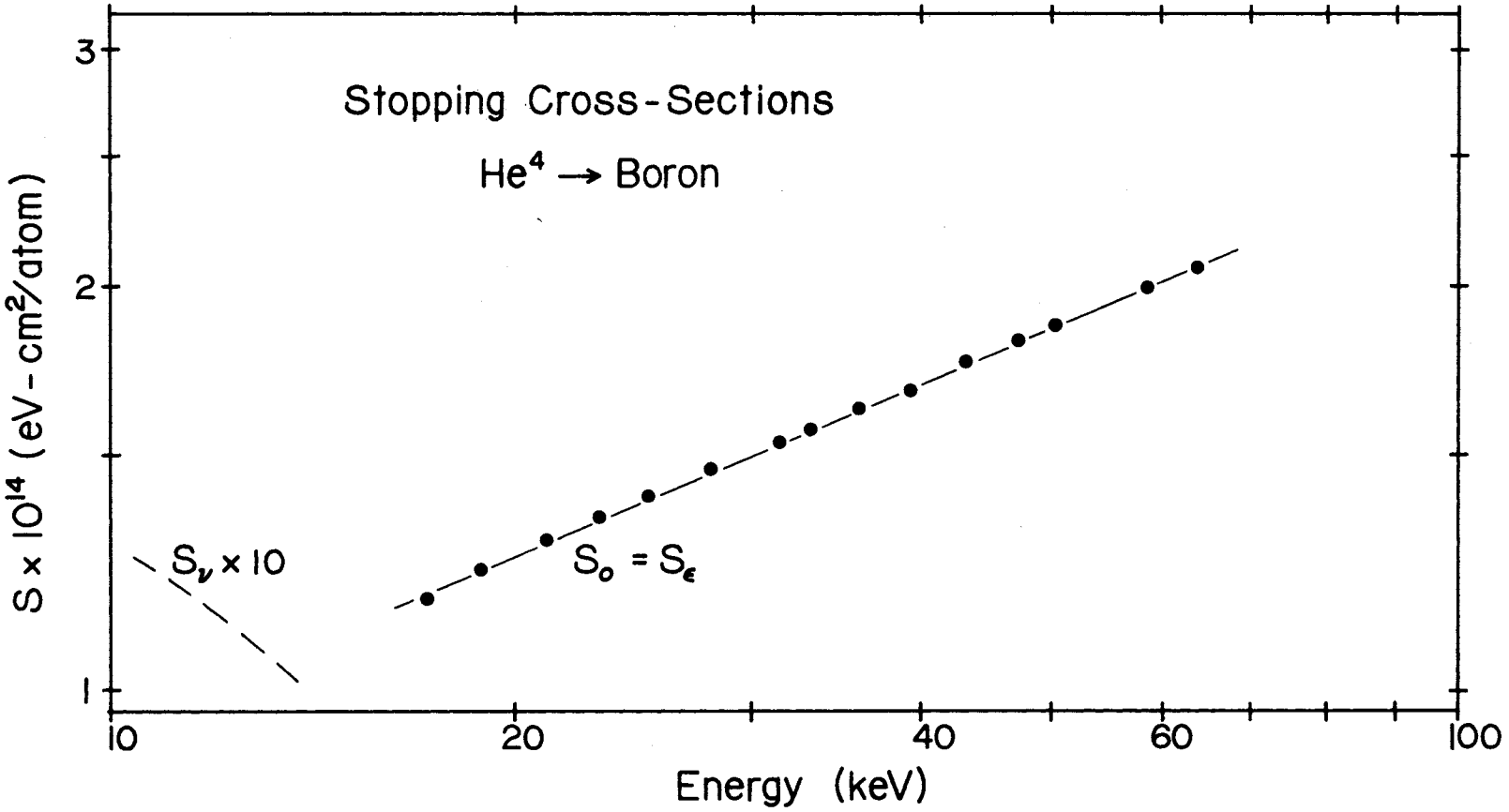
Stopping Cross-Sections
He⁴ → Boron
S x 10¹⁴ (eV-cm²/atom)
3
2
1
10
20
40
60
100
Energy (keV)
S_ν x 10
S_o = S_ε

FIG. 14

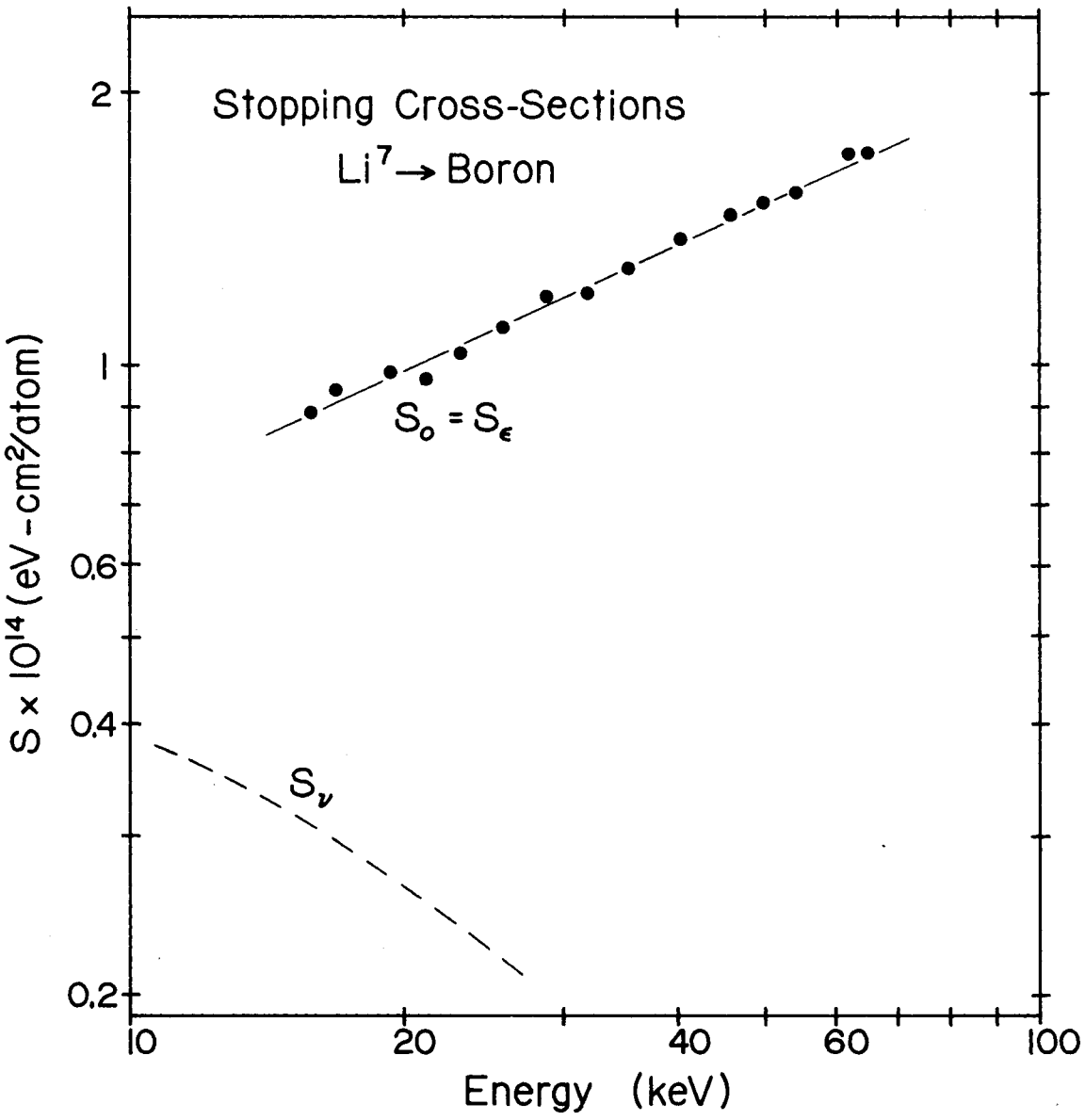
Stopping Cross-Sections
Li⁷ → Boron
S₀ = Sε
Sν
S x 10¹⁴ (eV-cm²/atom)
2
1
0.6
0.4
0.2
10
20
40
60
100
Energy (keV)

FIG. 15

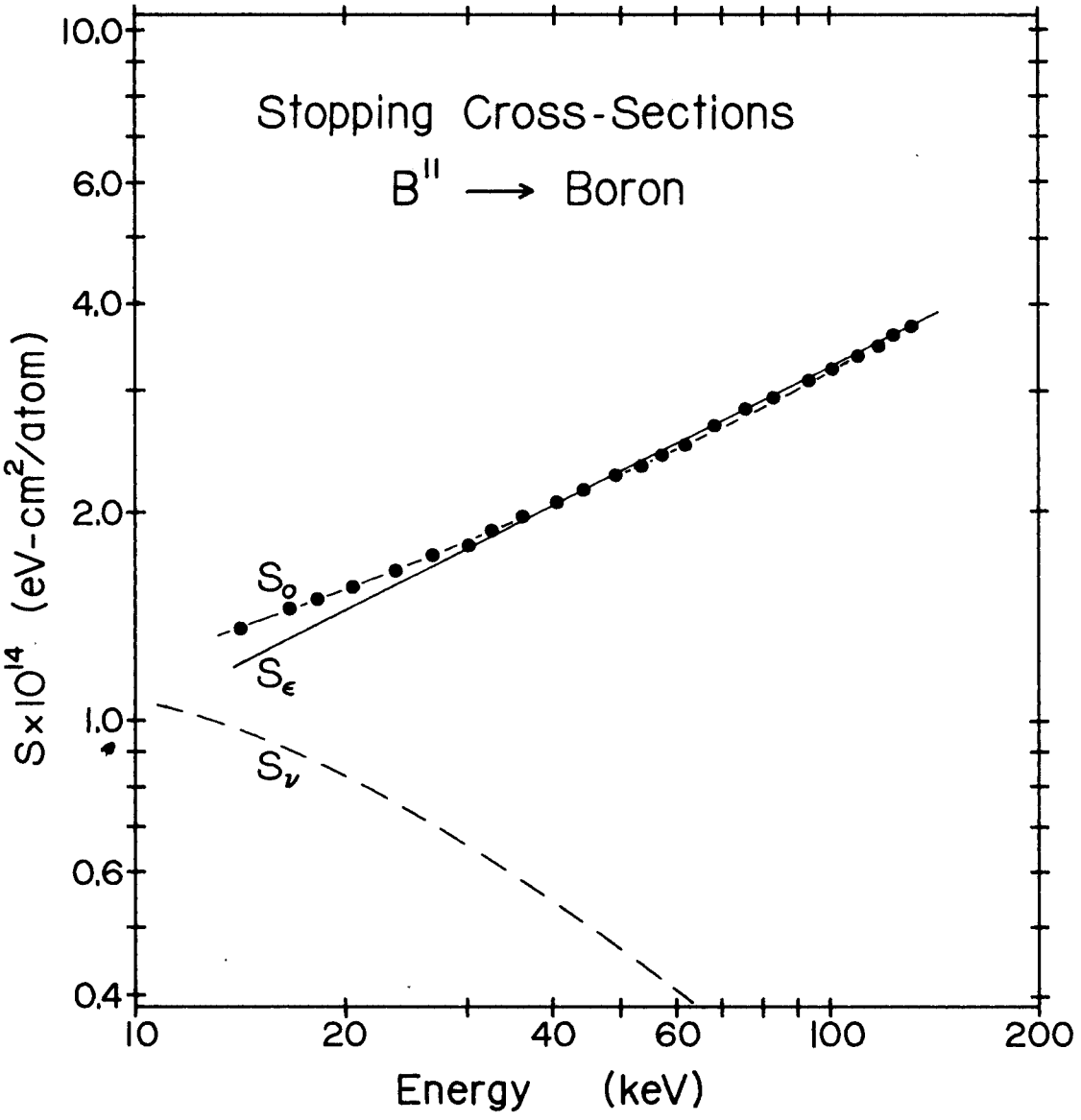
Stopping Cross-Sections
B11 → Boron
S×10^14 (eV-cm^2/atom)
10.0
6.0
4.0
2.0
1.0
0.6
0.4
10
20
40
60
100
200
Energy (keV)
S0
Sε
Sν

FIG. 16

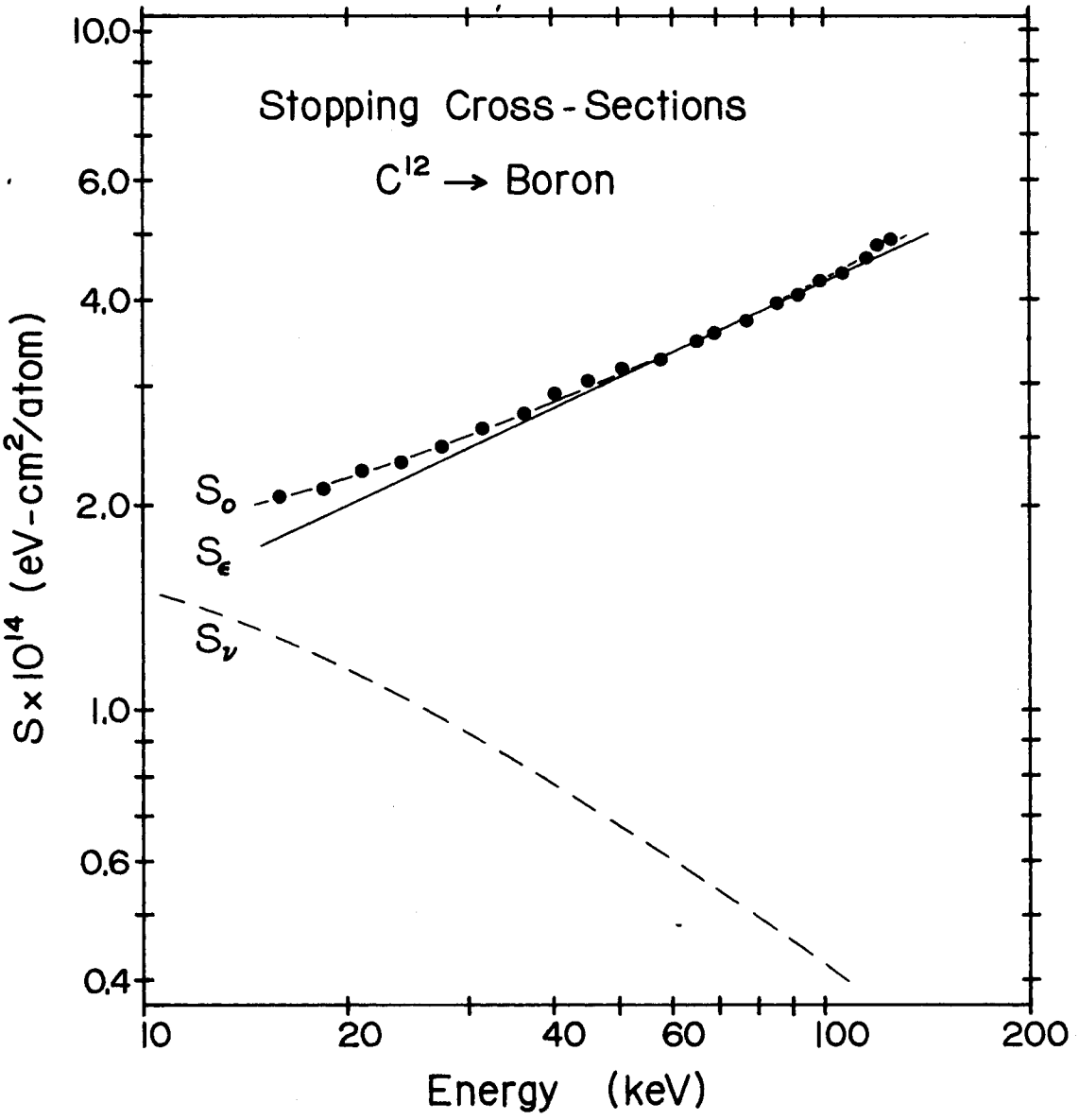
Stopping Cross-Sections
C^{12} → Boron
S_o
S_ϵ
S_ν
$S \times 10^{14}$ (eV-cm^2/atom)
10.0
6.0
4.0
2.0
1.0
0.6
0.4
10
20
40
60
100
200
Energy (keV)

FIG. 17

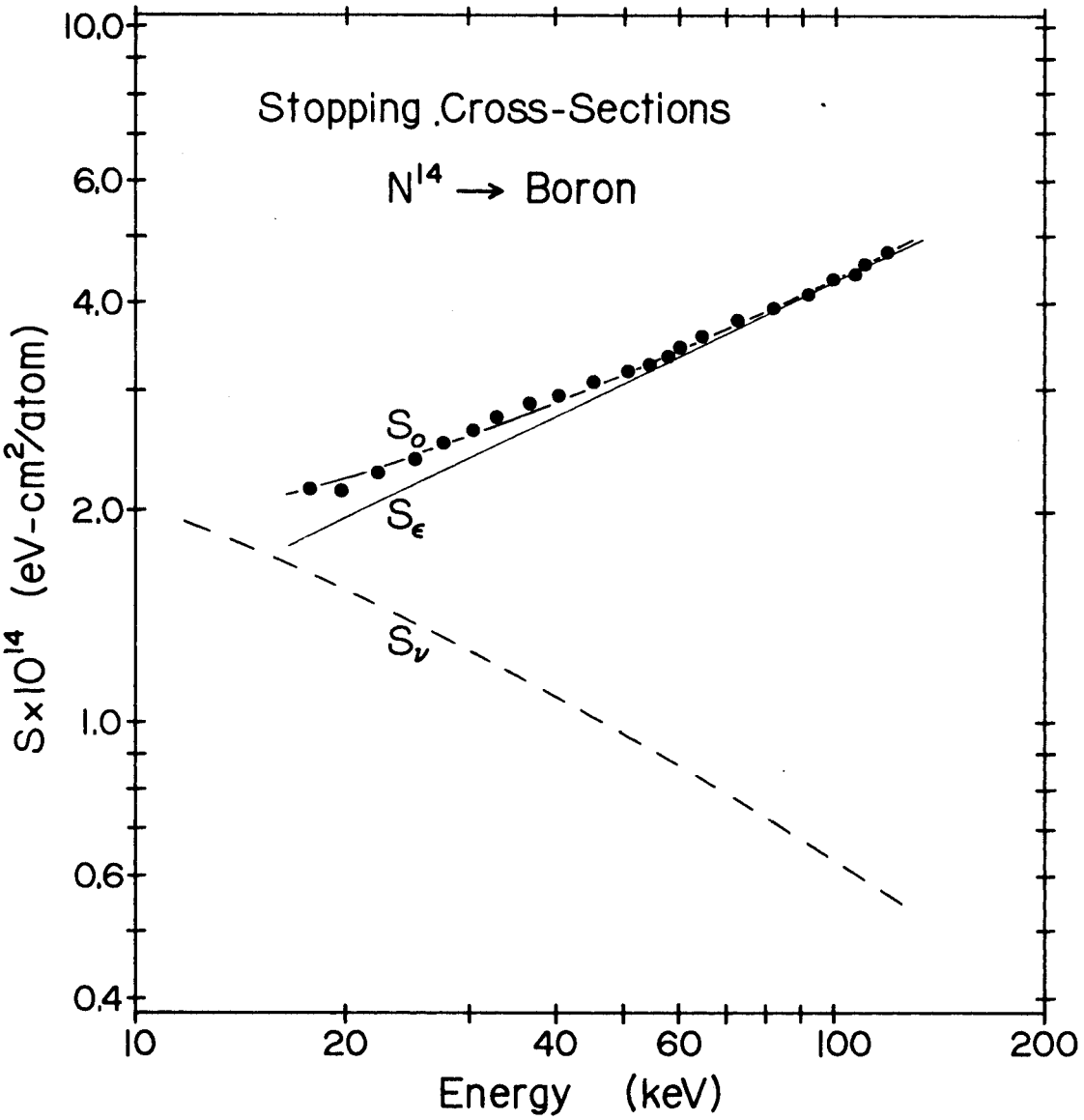
Stopping Cross-Sections
N14 → Boron
S0
Sε
Sν
S x 10^14 (eV-cm^2/atom)
10.0
6.0
4.0
2.0
1.0
0.6
0.4
10
20
40
60
100
200
Energy (keV)

FIG. 18

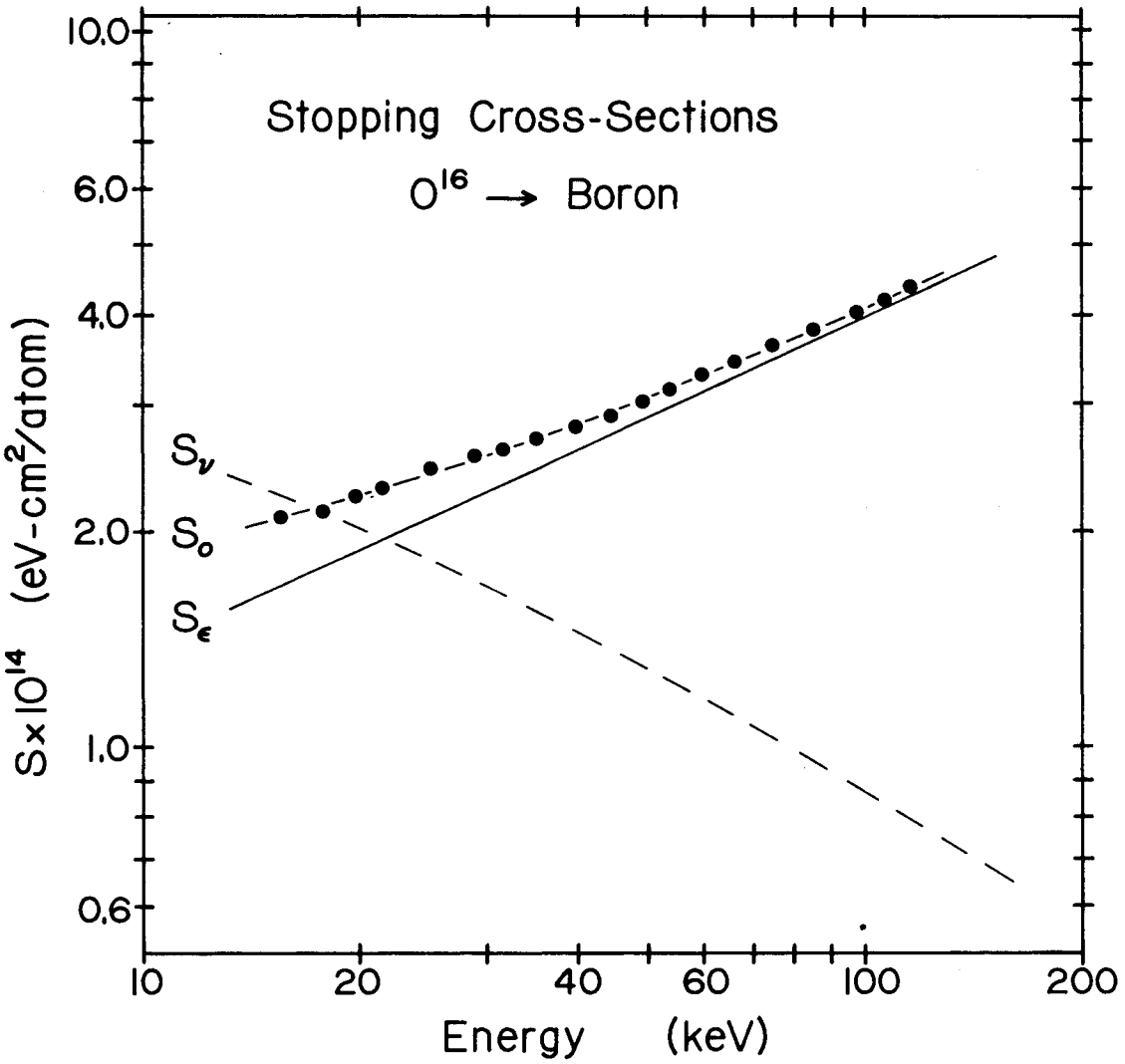
Stopping Cross-Sections
O^{16} → Boron
S_ν
S_o
S_ϵ
$S \times 10^{14}$ (eV-cm²/atom)
10.0
6.0
4.0
2.0
1.0
0.6
10
20
40
60
100
200
Energy (keV)

FIG. 19

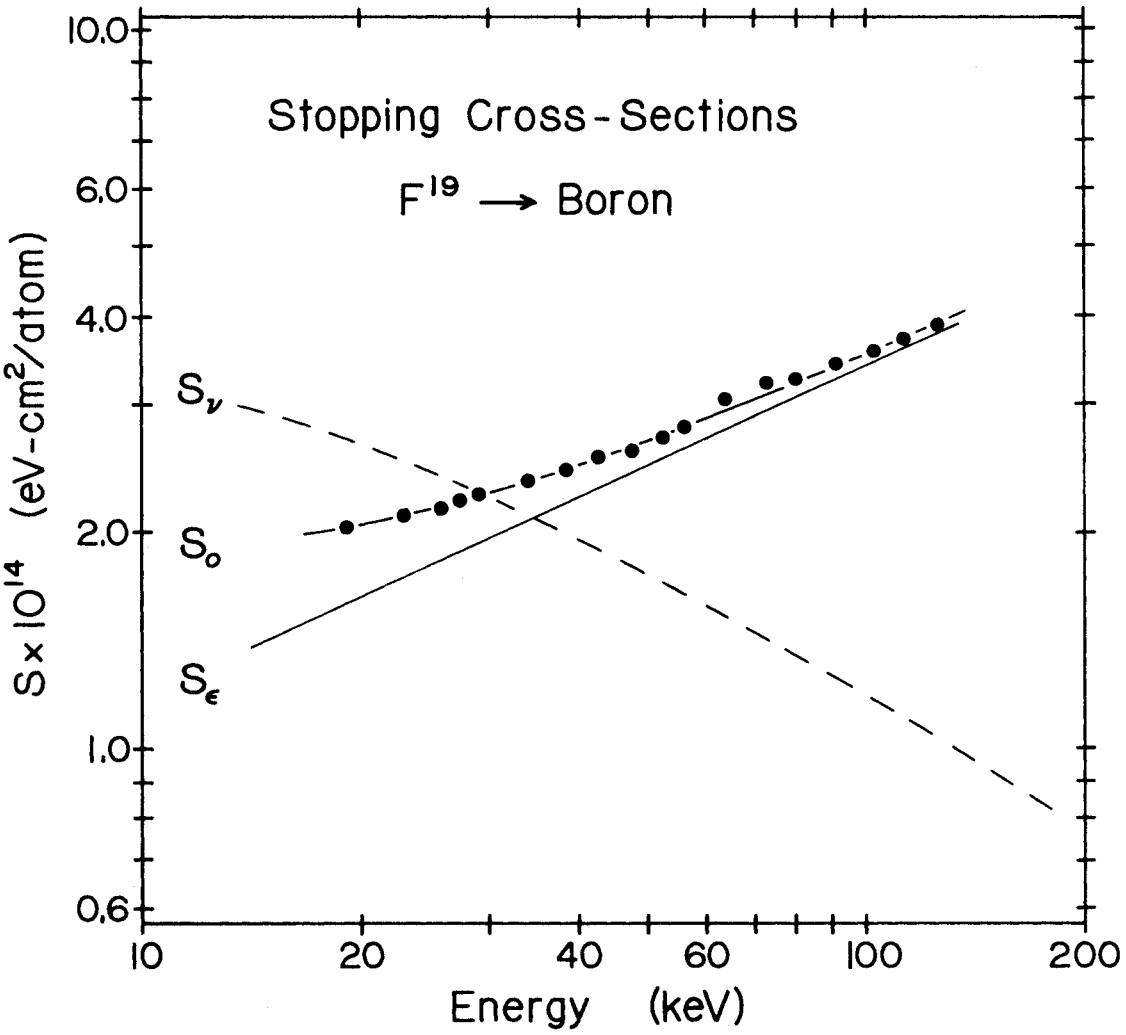
Stopping Cross-Sections
F19 → Boron
S × 10^14 (eV-cm^2/atom)
10.0
6.0
4.0
2.0
1.0
0.6
Sν
So
Sε
10
20
40
60
100
200
Energy (keV)

FIG. 20

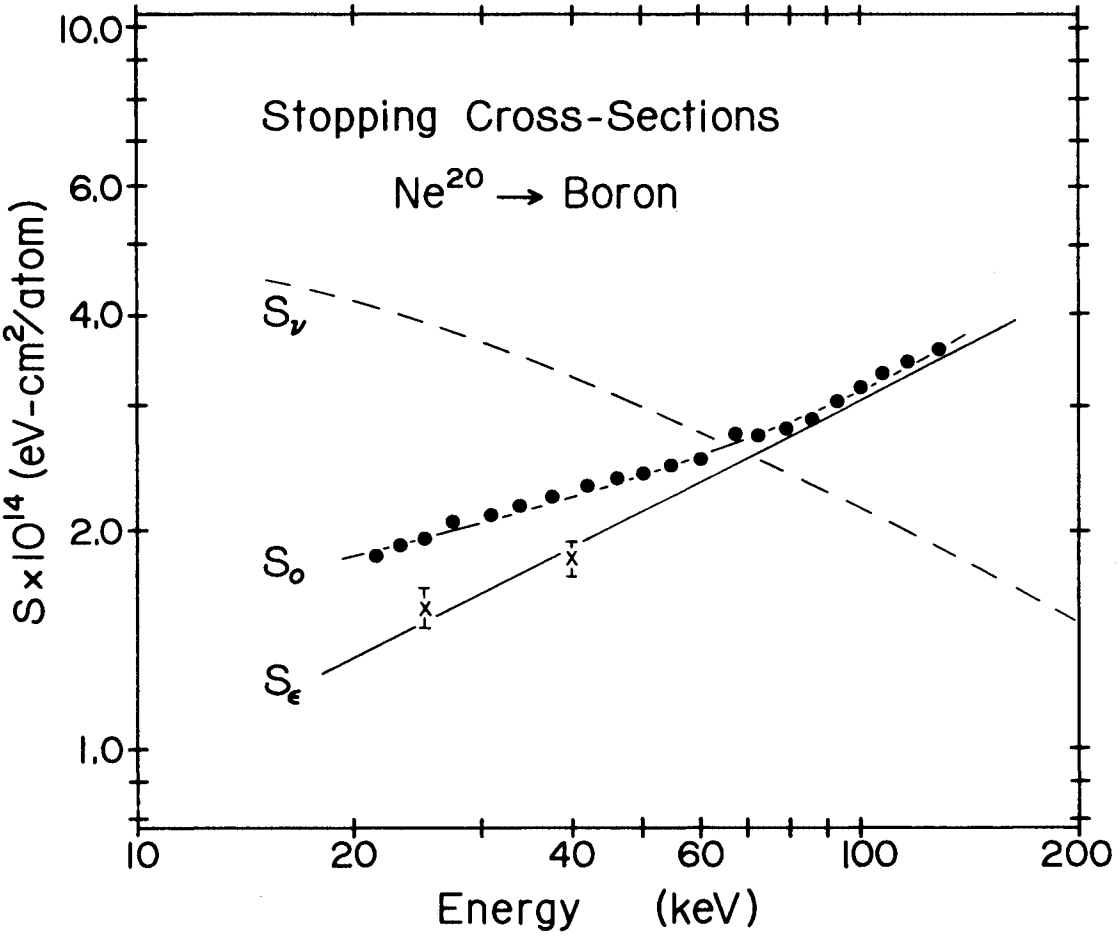
Stopping Cross-Sections
Ne20 → Boron
Sν
So
Sε
S x 10^14 (eV-cm^2/atom)
10.0
6.0
4.0
2.0
1.0
10
20
40
60
100
200
Energy (keV)

FIG. 21

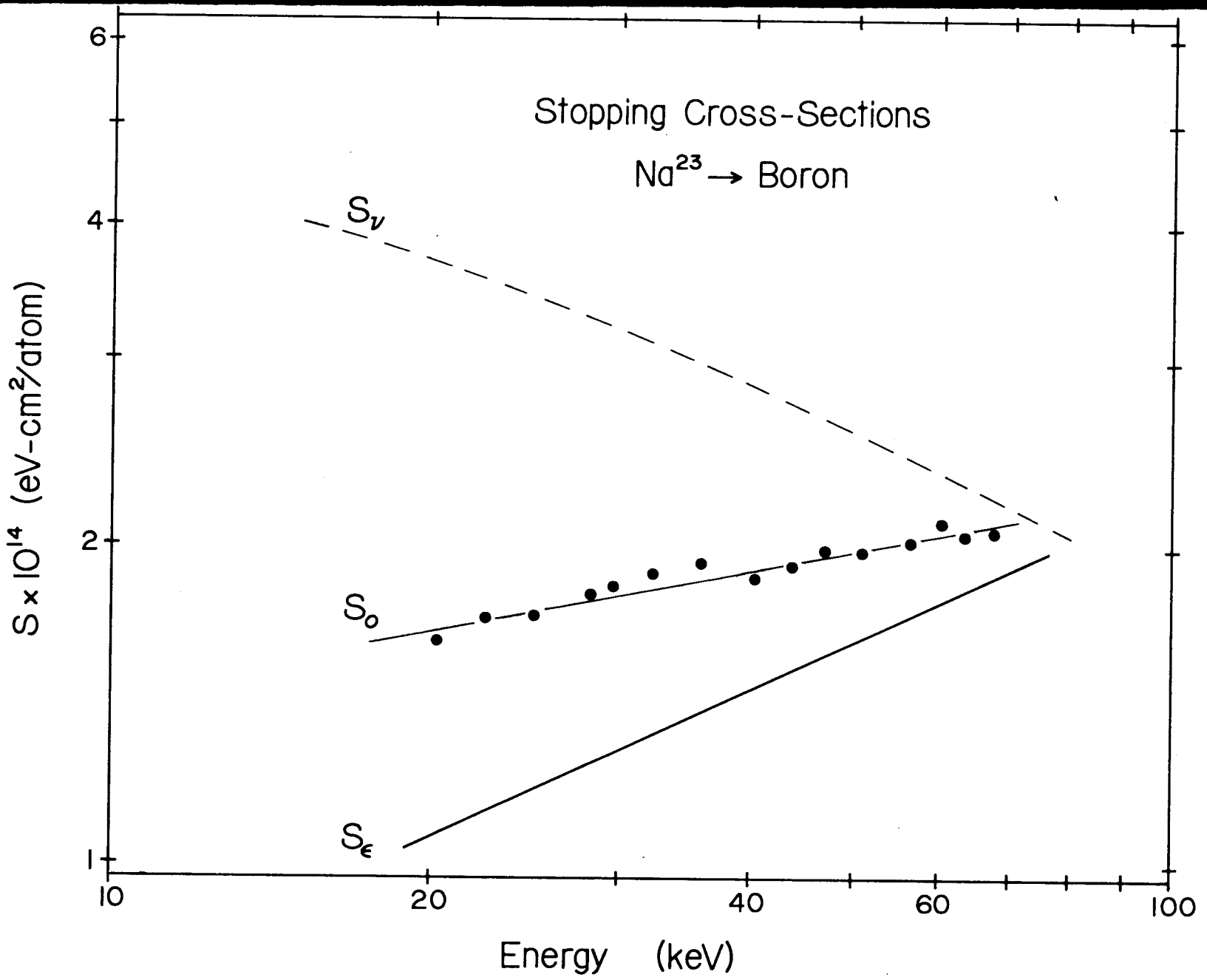
Stopping Cross-Sections
$Na^{23} \rightarrow$ Boron
S_v
S_o
S_ϵ
$S \times 10^{14}$ (eV-cm^2/atom)
6
4
2
1
10
20
40
60
100
Energy (keV)

FIG. 22

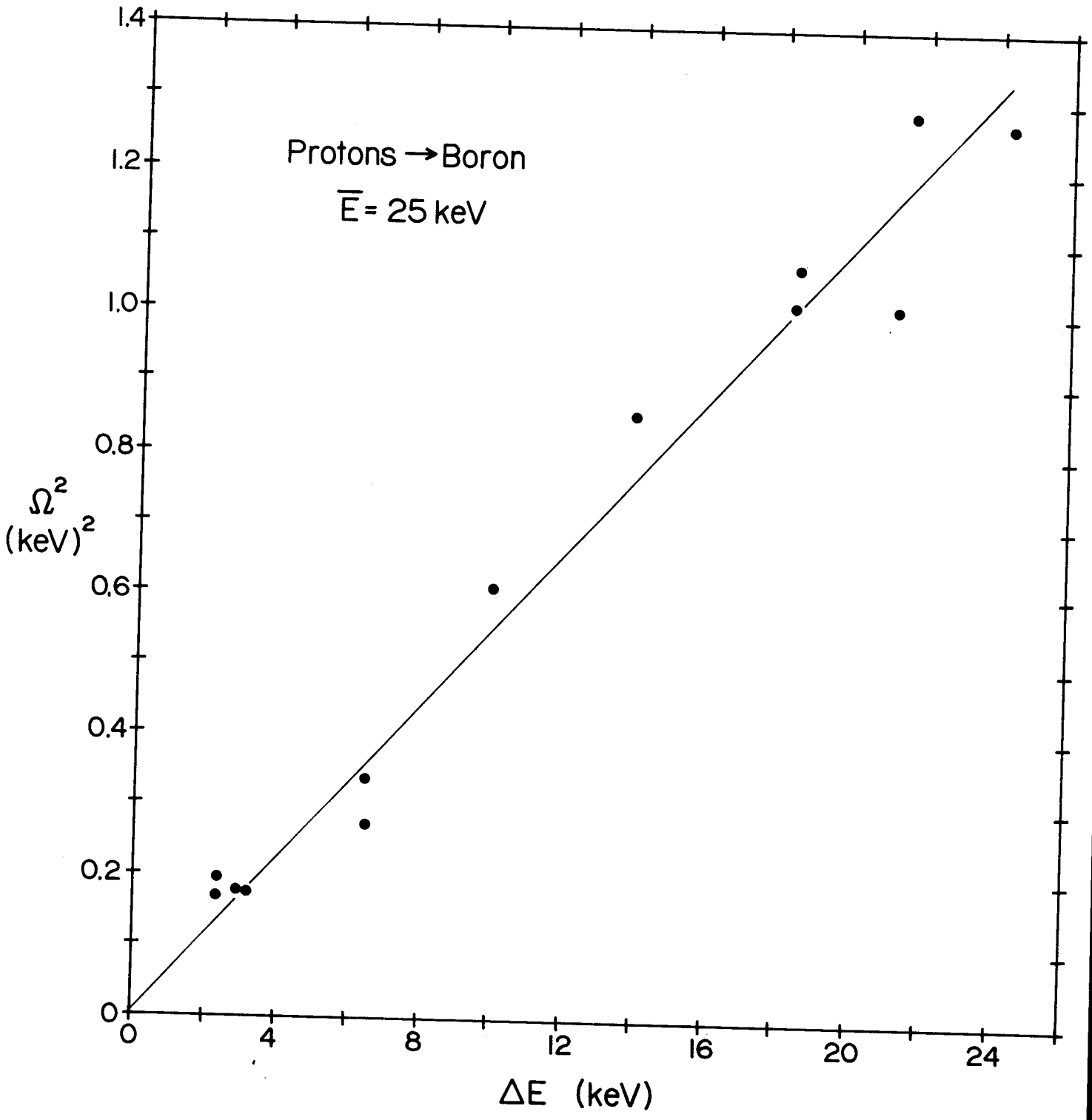
Protons → Boron
$\overline{E}$ = 25 keV
Ω^2
(keV)^2
1.4
1.2
1.0
0.8
0.6
0.4
0.2
0
0
4
8
12
16
20
24
ΔE (keV)

FIG. 23

CHAPTER V

DISCUSSION

1. Comparison with Other Experiments

The only comparison of our results using boron targets with those of others is for hydrogen projectiles. Overley and Whaling (O-62) have determined proton stopping cross-sections in boron for energies from 100 keV to 3 MeV. Their experimental points at 100 and 150 keV are shown as triangles in Fig. 24. Our hydrogen results are shown as dots at energies up to 64 keV in the same figure.

Because the energy separation between the two sets of results occurs in the region in which the energy dependence of the electronic stopping cross-section is in transition, no quantitative comparison of the results is possible. However, a qualitative comparison has been made, by matching the two sets of results with the dashed curve in Fig. 24. The smooth matching curve indicates that there is good agreement between the results of the present experiments and those of Overley and Whaling.

2. Comparison of Stopping Cross-Sections with Theory

Although the theory of the nuclear stopping process has been well developed (B-48, L-61, L-63), no comparison with it was possible because the results of our experiments were essentially electronic stopping cross-sections. However, the Monte Carlo correction for the nuclear component of the observed stopping cross-section, was based on the nuclear stopping

theory, and the good agreement between the calculations and the experimental angular distributions (Figures 5 and 6) and energy spectra (Fig. 7) provides a qualitative verification of the model used in the nuclear stopping theory.

The electronic stopping theory of Lindhard et al (L-61, L-63) is applicable for particle velocities less than $v_o \cdot Z_1^{2/3}$. Our experimental results can be compared with this theory at energies up to 25 keV, for hydrogen and at all energies for the other projectiles. The theoretical expression for the electronic stopping cross-section is given in equation I-9. Interesting comparisons can be made between experiment and theory regarding the energy dependence of S_ε, the values of S_ε for projectiles of different isotopes of the same element, and the variation of S_ε with the atomic number of projectiles and target atoms.

First we shall consider the energy dependence of S_ε. Equation I-9 predicts that the value of the energy exponent P is 0.5 in the empirical relation for the electronic stopping cross-section given in equation II-5. The experimental values of P range from 0.40 to 0.51. The agreement between theory and experiment is quite reasonable considering that the theory is based on a model in which the solid is represented by a degenerate electron gas.

The experimentally determined S_ε for protons has an energy exponent P = 0.40 valid at energies from 12-25 keV. Above 25 keV, S_ε approaches a maximum and then above 100 keV decreases with increasing energy (Fig. 24). This is in qualitative agreement with theory in the energy region in which the Lindhard prediction (Equation I-9) gives way to the well known Bloch theory at high energy. From the experimental

S_ε results with hydrogen shown in Fig. 24, the maximum in S_ε occurs at approximately 80 keV.

The Lindhard theory predicts that different isotopes of the same element having the same velocity, will have equivalent electronic stopping cross-sections. The experimental values of S_ε for protons and deuterons are shown in Fig. 24. The proton results (shown as solid dots) are those of Fig. 13, while the deuteron results (shown as open circles) are plotted with the energy scale contracted by a factor of two so that the isotopes would be compared at the same velocity. The theoretical prediction is verified inasmuch as a single smooth curve can be drawn through the experimental points for both isotopes.

The variation of S_ε with the atomic number of the projectile (Z_1) is shown in Fig. 25, in which S_ε has been plotted as a function of Z_1 at a particle velocity of 9×10^7 cm/sec. This velocity has no particular significance, but it is the velocity at which comparisons of S_ε with Z_1 were made in carbon, aluminum, and nickel targets (0-63, 0-64). All the projectiles but H^1 and Na^{23} were studied at this velocity, and the values of S_ε were taken from the graphs of the experimental results (Fig. 14-21) at the appropriate energies. For H^1 and Na^{23}, the S_ε results at this velocity represent extrapolations beyond the experimental energy domain using equation II-5 and values of k and P from Table IV-1.

The lines drawn on the graph in Fig. 25 are solutions to equation I-9. The central line corresponds to $\zeta_\varepsilon = Z_1^{1/6}$ while the two outside lines are the limits of the theoretical prediction with $\zeta_\varepsilon = 1$ and 2, respectively.

A periodic dependence of S_ε on the atomic number of the projectile, as was found in carbon, aluminum, and nickel (O-63, O-64), is also seen in Fig. 25 for boron targets. The value of S_ε rises to a maximum at $Z_1 \simeq 8$, then decreases as Z_1 increases to 11. A slight discontinuity appears at $Z_1 \simeq 3$. This shape of the periodic variation is the same as that found in the other target materials. The theory of Lindhard et al with $\zeta_\varepsilon = Z_1^{1/6}$ in equation I-9, predicts the general trend of the experimental results, but does not include the periodic variation of S_ε with Z_1.

A theoretical treatment of the electronic stopping process based on Thomas-Fermi arguments can not be expected to explain in detail the variations with atomic number of either target or projectile atoms. The statistical nature of the model neglects the periodic properties of the outer electrons in the atoms. It is to be expected that the periodic nature of S_ε will be explained in detail only when the binding of the last few electrons is taken into account in the theoretical treatment of the stopping process.

An interesting aspect of equation I-9 is the symmetry in the atomic number of target and projectile atoms. That is, S_ε is predicted to be independent of an interchange of the target and projectile materials as long as the projectiles are kept at the same velocity. Our results with $C^{12} \rightarrow$ Boron and those of Ormrod (O-63) with $B^{11} \rightarrow$ Carbon are shown in Fig. 26. The results with carbon projectiles have been shifted to higher energy from those shown in Fig. 17, in order to make a comparison at the same projectile velocity. S_o is approximately 7% larger for carbon than for boron projectiles at the energies for which $S_o = S_\varepsilon$.

However, this does not represent any major disagreement with the theoretical prediction, since close agreement between the two sets of results would have been fortuitous in view of the periodic variation of S_ε with Z_1.

3. Comparison of Straggling with Theory

The experimentally determined straggling can be compared with the straggling theory of Lindhard (L-54) in terms of the variation in proton straggling with film thickness, and the magnitudes of the relative straggling of hydrogen and helium projectiles.

First, the prediction of equation I-10 is that Ω^2 is directly proportional to ΔE for particles having the same velocity. In our experiments, this means that Ω^2 and ΔE are expected to have the same dependence on film thickness. Experiments were performed with protons in films of various thickness, and a plot of Ω^2 versus ΔE was given in Fig. 23. The best straight line through the origin and the experimental points was determined by a least squares analysis. Ten of the thirteen experimental points lie within one probable error of the line, and we conclude that the relative straggling is independent of film thickness in good agreement with the theoretical prediction.

The relative straggling given in equation I-10 depends upon the electron density (n_ε) in the degenerate electron gas model. In making comparison with experiment, values of $\frac{\Omega^2}{\Delta E}$ were calculated using three values of n_ε corresponding to:

1) the atomic density $N = 1.30 \times 10^{23}$ cm^{-3} for boron.

2) the number of valence electrons $3N$.

3) the total electron density in the solid $5N$.

The best value of n_ϵ is expected to be between the limits of 1) and 3) and possibly equal to 2). The calculated and experimental values of $\frac{\Omega^2}{\Delta E}$ are given in Table V-1.

4. Summary

Stopping cross-sections have been determined in thin boron films for atomic projectiles ($Z \leq 11$) with energies ranging from 10-140 keV.

The absolute value of the stopping cross-section of protons in boron was found using thick weighed films. This result was used to determine the thickness of the films used in the experiments.

The electronic stopping-cross sections have been obtained by correcting the observed stopping cross-sections for the nuclear component. This was done using a Monte Carlo calculation developed by Ormrod (O-63).

The relative straggling in energy has been determined for hydrogen and helium projectiles in boron films.

Comparison has been made between the experimental results and the theoretical predictions of Lindhard et al (L-54, L-61, L-63). In general, the agreement is good. However, an observed periodic dependence of S_ϵ upon Z_1 is not explained by the theory.

TABLE V-1

Comparison Between Experimental and Theoretical Values of the Relative Straggling in Boron

Projectile Velocity	Experimental Value of $\frac{\Omega^2}{\Delta E}$		Calculated Value of $\frac{\Omega^2}{\Delta E}$ from equation I-10		
	$H^1 \rightarrow$ Boron	$He^4 \rightarrow$ Boron	1) $n_\xi = N$	2) $n_\xi = 3N$	3) $n_\xi = 5N$
$v = v_o$	0.055±5%		0.043	0.057	0.064
$v = 0.5\ v_o$		0.054±12%	0.021	0.028	0.032

The agreement between experimental and calculated values of the proton straggling is excellent.

Although the agreement found for the helium projectiles is not as good as for the protons, it is quite reasonable in view of the approximate nature of equation I-10.

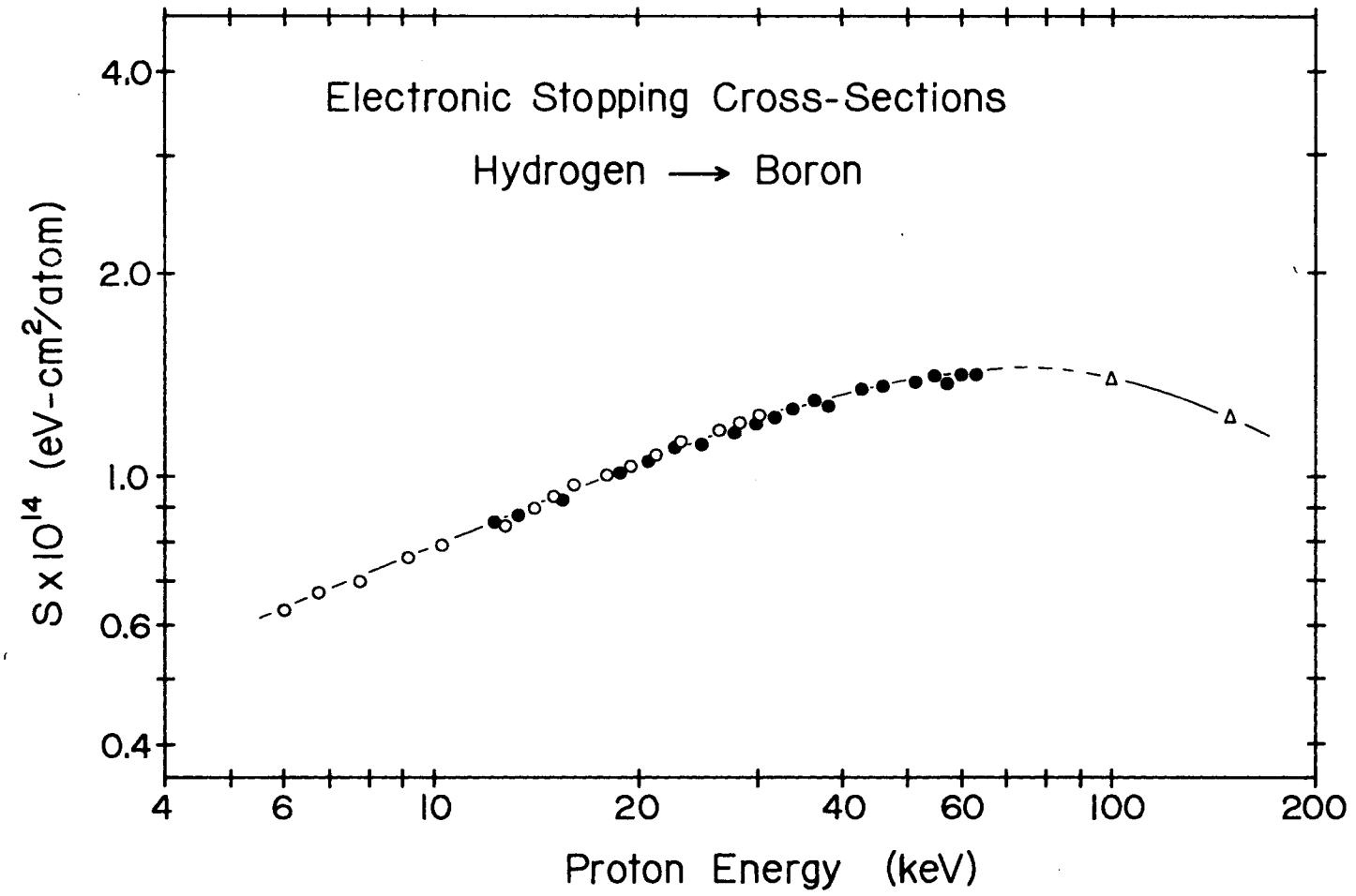
Electronic Stopping Cross-Sections
Hydrogen → Boron
S x 10^14 (eV-cm^2/atom)
4.0
2.0
1.0
0.6
0.4
4
6
10
20
40
60
100
200
Proton Energy (keV)

FIG. 24

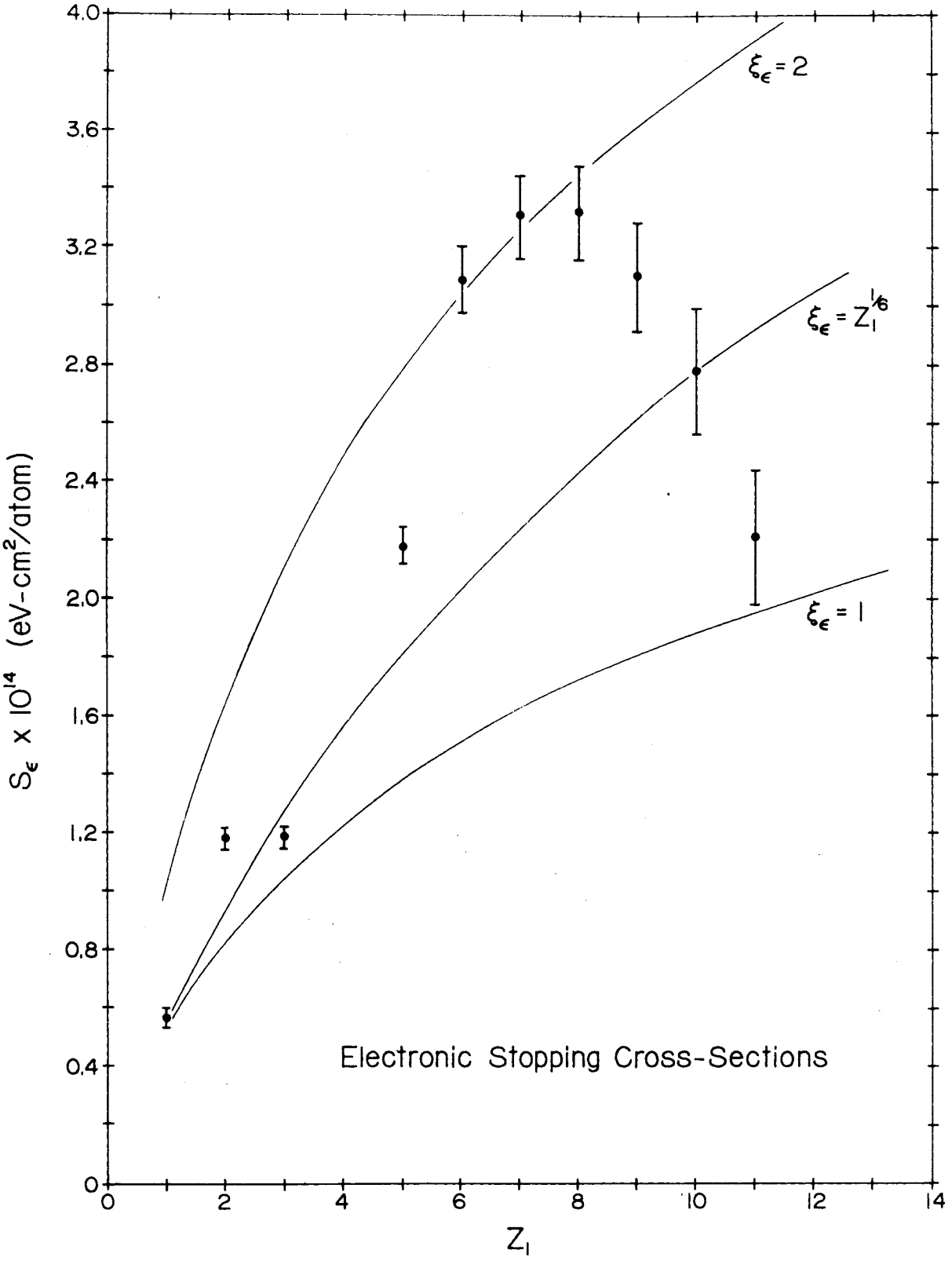
Electronic Stopping Cross-Sections
$S_\epsilon \times 10^{14}$ (eV-cm²/atom)
Z_1
$\xi_\epsilon = 2$
$\xi_\epsilon = Z_1^{1/6}$
$\xi_\epsilon = 1$
0
0.4
0.8
1.2
1.6
2.0
2.4
2.8
3.2
3.6
4.0
0
2
4
6
8
10
12
14

FIG. 25

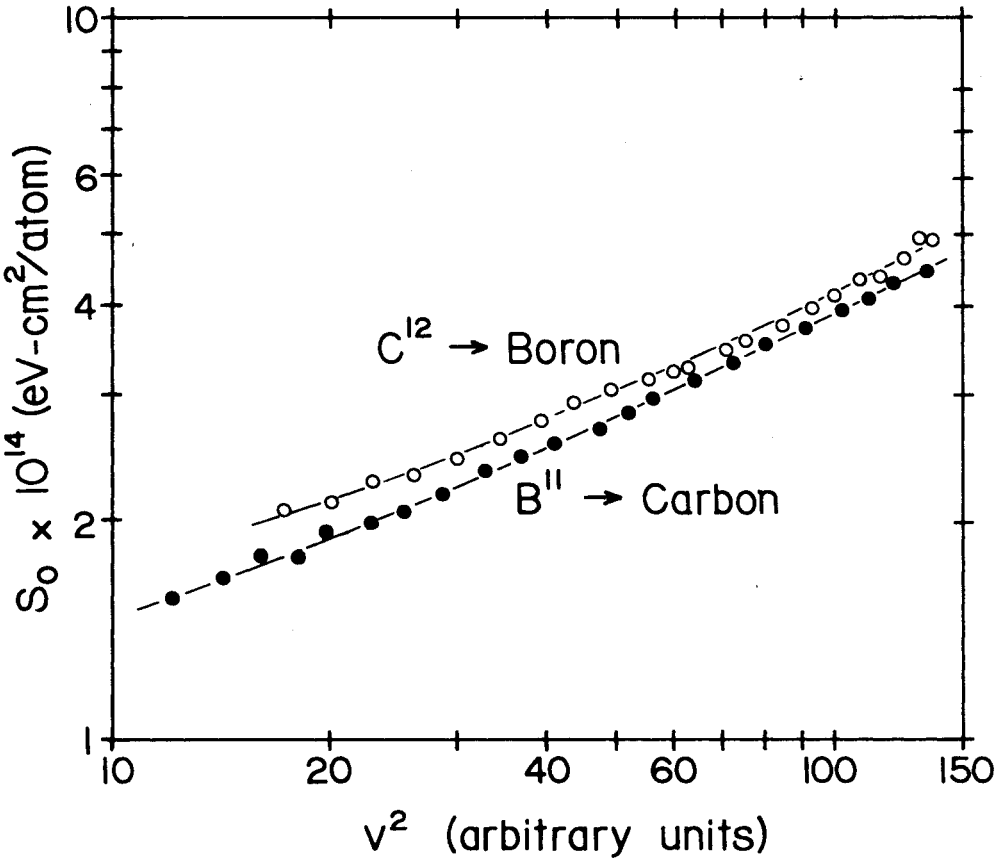
10
6
4
2
1
$S_o \times 10^{14}$ (eV-cm^2/atom)
C^{12} → Boron
B^{11} → Carbon
10
20
40
60
100
150
v^2 (arbitrary units)

FIG. 26

REFERENCES

(A-53) S.K. Allison and S.D. Warshaw, Rev. Mod. Phys. 25, 779 (1953).

(A-62) H.L. Adair and E.H. Kobisk, Trans. 9th National Vacuum Symposium, American Vacuum Society (1962).

(B-33) F. Bloch, Ann. Physik. 16, 285 (1933).

(B-36) R. Beeching, Electron Diffraction, Methuen and Co., London (1936).

(B-48) Niels Bohr, K. Dansk. Videnskab. Selskab Matt. Fys. Medd. 18, #8 (1948).

(E-55) E. Everhart, G. Stone, and R. Carbone, Phys. Rev. 99, 1287 (1955).

(F-47) E. Fermi and E. Teller, Phys. Rev. 72, 399 (1947).

(F-58) O.B. Firsov, J.E.T.P. 7, 308 (1958).

(L-54) J. Lindhard, K. Dansk. Videnskab. Selskab Matt. Fys. Medd. 28, #8 (1954).

(L-61) J. Lindhard and M. Scharff, Phys. Rev. 124, 128 (1961).

(L-63) J. Lindhard, M. Scharff, and H.E. Schiott, K. Dansk. Videnskab. Selskab Matt. Fys. Medd. 33, #14 (1963).

(M-61) A.H.F. Muggleton and F.A. Howe, Nucl. Inst. and Meth. 13, 211 (1961).

(N-63) L.C. Northcliffe, To appear in Ann. Rev. Nucl. Sci.

(O-62) J.C. Overley and W. Whaling, Phys. Rev. 128, 315 (1962).

(O-63) J.H. Ormrod and H.E. Duckworth, Can. J. Phys. 41, 1424 (1963).

(O-63A) J.H. Ormrod, Thesis, McMaster University (1963).

(O-64) J.H. Ormrod, J.R. Macdonald, and H.E. Duckworth, To be published.

(R-11) E. Rutherford, Phil. Mag. 21, 669 (1911).

(S-61) G.N. Strivastava and G.D. Scott, Brit. J. Appl. Phys. 12, 255 (1961).

(W-58) W. Whaling, Handbuch der Physik XXXIV, 193 (1958).

(W-62) A. Van Wijngaarden and H.E. Duckworth, Can. J. Phys. 40, 1749 (1962).

(W-62A) A. Van Wijngaarden, Thesis, McMaster University (1962).

(Y-62) L. Yaffé, Ann. Rev. Nucl. Sci. 12, 153 (1962).